الجمهورية الجزائرية الديمقراطية الشعبية
PEOPLE'S DEMOCRATIC REPUBLIC OF ALGERIA
وزارة التعليم العالي والبحث العلمي
MINISTRY OF HIGHER EDUCATION AND SCIENTIFIC RESEARCH
جامعة الجلفة
UNIVERSITY OF DJELFA
كلية العلوم الدقيقة والاعلام الالي
Faculty of the Exact Science and Computer Science
قسم الفيزياء
Department of physics

Course of

FIBER OPTICS and LASERS

Second year Master's students
Major: Energétique et énergie renouvelable

Elaborated by:
Dr. LAHOUAL Mohamed

University year: 2023-2024

Contents

Part I
Fiber Optics

Chapter I
Electromagnetics and Optics

1.1 Introduction

the study of the propagation of light in any medium requires a knowledge of maxwell's equations. In this chapter, we will briefly discuss the basics of laws of electromagnetics leading to Maxwell's equations. Maxwell's equations will be used to derive the wave equation, which forms the basis for the study of optical fibers in Chapter 2. The results derived in this chapter will be used throughout the courses.

1.2 Maxwell's Equations

$$div\ D = \rho$$

$$div\ B = 0$$

$$\nabla \times E = -\frac{\partial B}{\partial t}$$

$$\nabla \times H = J + \frac{\partial D}{\partial t}$$

From above equations, we see that a time-changing magnetic field produces an electric field and a time-changing electric field or current density produces a magnetic field. The charge distribution ρ and current density J are the *sources* for generation of electric and magnetic fields. For the given charge and current distribution, the equations may be solved to obtain the electric and magnetic field distributions. The terms on the right-hand sides of third and fourth equations may be viewed as the sources for generation of field intensities appearing on the left-hand sides of the same equations. As an example, consider the alternating current $I_0 \sin(2\pi f t)$ flowing in the transmitter antenna. From Ampere's law, we find that the current leads to a magnetic field intensity around the antenna (first term of the fourth equation. From Faraday's law, it follows that the time-varying magnetic field induces an electric field intensity (third equation) in the vicinity of the antenna.

Consider a point in the neighborhood of the antenna (but not on the antenna). At this point $J = 0$, but the time-varying electric field intensity or displacement current density (second term on the right-hand side of (fourth Equation) leads to a magnetic field intensity, which in turn leads to an electric field intensity (third equation). This process continues and the generated electromagnetic wave propagates outward just like the water wave generated by throwing a stone into a lake. If the displacement current density were to be absent, there would be no continuous coupling between electric and magnetic fields and we would not have had electromagnetic waves.

1.2.1 Maxwell's Equation in a Source-Free Region

In free space or dielectric, if there is no charge or current in the neighborhood, we can set $\rho = 0$ and $J = 0$ in Eqs. (1.1) and (1.4). Note that the above equations describe the relations between electric field, magnetic field, and the sources at a space-time point and therefore, in a region sufficiently far away from the sources, we can set $\rho = 0$ and $J = 0$ in that region. However, on the antenna, we cannot ignore the source terms ρ or J in Eqs. (1.1-1.4). Setting $\rho = 0$ and $J = 0$ in the source-free region, Maxwell's equations take the form

$$div\, D = 0 \tag{1.1}$$

$$div\, B = 0 \tag{1.2}$$

$$\nabla \times E = -\frac{\partial B}{\partial t} \tag{1.3}$$

$$\nabla \times H = \frac{\partial D}{\partial t} \tag{1.4}$$

In the source-free region, the time-changing electric/magnetic field (which was generated from a distant source ρ or J) acts as a *source* for a magnetic/electric field.

1.2.2 Electromagnetic Wave

Suppose the electric field is only along the *x*-direction,

$$E = E_x x \tag{1.5}$$

and the magnetic field is only along the *y*-direction,

$$H = H_y y \tag{1.6}$$

Substituting Eqs. (1.5) and (1.6) into Eq. (1.3), we obtain

$$\nabla \times E = \begin{bmatrix} x & y & z \\ \frac{\partial}{\partial x} & \frac{\partial}{\partial y} & \frac{\partial}{\partial z} \\ E_x & 0 & 0 \end{bmatrix} = \frac{\partial E_x}{\partial z} y - \frac{\partial E_x}{\partial y} z = -\mu \frac{\partial H_y}{\partial t} y \tag{1.7}$$

Equating *y*- and *z*-components separately, we find

$$\frac{\partial E_x}{\partial z} = -\mu \frac{\partial H_y}{\partial t} \tag{1.8}$$

$$\frac{\partial E_x}{\partial y} = 0 \tag{1.9}$$

Substituting Eqs. (1.5) and (1.6) into Eq. (1.4), we obtain

$$\nabla \times E = \begin{bmatrix} x & y & z \\ \frac{\partial}{\partial x} & \frac{\partial}{\partial y} & \frac{\partial}{\partial z} \\ 0 & H_y & 0 \end{bmatrix} = \frac{\partial H_y}{\partial z} x + \frac{\partial H_y}{\partial x} z = \varepsilon \frac{\partial E_x}{\partial t} x \tag{1.10}$$

Therefore,

$$\frac{\partial H_y}{\partial z} = -\varepsilon \frac{\partial E_x}{\partial t} \tag{1.11}$$

$$\frac{\partial H_y}{\partial x} = 0 \tag{1.12}$$

Eqs. (1.8) and (1.11) are coupled. To obtain an equation that does not contain *Hy*, we differentiate Eq. (1.8) with respect to *z* and differentiate Eq. (1.11) with respect to *t*,

$$\frac{\partial^2 E_x}{\partial z^2} = -\mu \frac{\partial H_y}{\partial t \partial z} \tag{1.13}$$

$$\mu \frac{\partial^2 H_y}{\partial t \partial z} = -\mu\varepsilon \frac{\partial E_x}{\partial t^2} \tag{1.14}$$

Adding Eqs. (1.13) and (1.14), we obtain

$$\frac{\partial^2 E_x}{\partial z^2} = \mu\varepsilon \frac{\partial E_x}{\partial t^2} \tag{1.15}$$

The above equation is called the *wave equation* and it forms the basis for the study of electromagnetic wave propagation.

1.2.3 Free-Space Propagation

For free space,$\varepsilon = \varepsilon_0 = 8.854 \times 10^{-12} C^2/Nm^2$, $\mu = \mu_0 = 4\pi \times 10^{-7} N/A^2$, and

$$c = \frac{1}{\sqrt{\mu_0 \varepsilon_0}} \simeq 3 \times 10^8 m/s \tag{1.16}$$

where *c* is the velocity of light in free space. Before Maxwell's time, electrostatics, magnetostatics, and optics were unrelated. Maxwell unified these three fields and showed that the light wave is actually an electromagnetic wave with velocity given by Eq. (1.16).

1.2.4 Propagation in a Dielectric Medium

Similar to Eq. (1.16), the velocity of light in a medium can be written as

$$v = \frac{1}{\sqrt{\mu\varepsilon}} \tag{1.17}$$

Where $\mu = \mu_0\mu_r$ and $\varepsilon = \varepsilon_0\varepsilon_r$. Therefore,

$$v = \frac{1}{\sqrt{\mu_0\mu_r\,\varepsilon_0\varepsilon_r}} \tag{1.18}$$

Using Eq. (1.17) in Eq. (1.18), we have

$$v = \frac{c}{\sqrt{\mu_r\,\varepsilon_r}} \tag{1.19}$$

For dielectrics, $\mu_r = 1$ and the velocity of light in a dielectric medium can be written as

$$v = \frac{c}{\sqrt{\varepsilon_r}} = \frac{c}{n} \tag{1.20}$$

where $n = \sqrt{\varepsilon_r}$ is called the refractive index of the medium. The refractive index of a medium is greater than 1 and the velocity of light in a medium is less than that in free space.

1.3.1-Dimensional Wave Equation

Using Eq. (1.17) in Eq. (1.15), we obtain

$$\frac{\partial^2 E_x}{\partial z^2} = \frac{1}{v^2}\frac{\partial^2 E_x}{\partial t^2} \tag{1.21}$$

Elimination of E_x from Eqs. (1.8) and (1.11) leads to the same equation for H_y,

$$\frac{\partial^2 H_y}{\partial z^2} = \frac{1}{v^2}\frac{\partial^2 H_y}{\partial t^2} \tag{1.22}$$

To solve Eq. (1.21), let us try a trial solution of the form

$$E_x(t, z) = f(t + \alpha z) \tag{1.23}$$

where f is an arbitrary function of $t + \alpha z$. Let

$$u = t + \alpha z \tag{1.24}$$

$$\frac{\partial u}{\partial z} = \alpha, \frac{\partial u}{\partial t} = 1 \tag{1.25}$$

$$\frac{\partial E_x}{\partial z} = \frac{\partial E_x}{\partial u}\frac{\partial u}{\partial z} = \frac{\partial E_x}{\partial u}\alpha \tag{1.26}$$

$$\frac{\partial^2 E_x}{\partial z^2} = \frac{\partial^2 E_x}{\partial u^2}\alpha^2 \tag{1.27}$$

$$\frac{\partial^2 E_x}{\partial t^2} = \frac{\partial^2 E_x}{\partial u^2} \tag{1.28}$$

Using Eqs. (1.27) and (1.28) in Eq. (1.21), we obtain

$$\alpha^2 \frac{\partial^2 E_x}{\partial u^2} = \frac{1}{v^2}\frac{\partial^2 E_x}{\partial u^2} \tag{1.29}$$

Therefore,

$$\alpha = \pm\frac{1}{v} \tag{1.30}$$

$$E_x = f\left(t + \frac{z}{v}\right) \text{ or } E_x = f\left(t - \frac{z}{v}\right) \tag{1.31}$$

The negative sign implies a forward-propagating wave and the positive sign indicates a backward-propagating wave. Note that *f* is an arbitrary function and it is determined by the initial conditions as illustrated by the following examples.

1.3.1 1-Dimensional Plane Wave

A plane wave can be written in any of the following forms:

$$E_x(t, z) = E_{x0} cos\left[2\pi f\left(t - \frac{z}{v}\right)\right]$$
$$E_x(t, z) = E_{x0} cos\left[2\pi f t - \frac{2\pi}{\lambda} z\right]$$

$$E_x(t,z) = E_{x0}cos(\omega t - kz) \tag{1.32}$$

where υ is the velocity of light in the medium, f is the frequency, $\lambda = \upsilon/f$ is the wavelength, $\omega = 2\pi f$ is the angular frequency, $k = 2\pi/\lambda$ is the wavenumber, and k is also called the propagation constant. Frequency and wavelength k are related by

$$\upsilon = f\lambda \tag{1.33}$$

or equivalently

$$\upsilon = \frac{\omega}{k} \tag{1.34}$$

Since H_y also satisfies the wave equation Eq. (1.22), it can be written as

$$H_y(t,z) = H_{y0}cos(\omega t - kz) \tag{1.35}$$

From Eq. (1.11), we have

$$\frac{\partial H_y}{\partial z} = -\varepsilon\frac{\partial E_x}{\partial t} \tag{1.36}$$

Using Eq. (1.32) in Eq. (1.36), we obtain

$$\frac{\partial H_y}{\partial z} = \varepsilon\omega H_{y0}cos(\omega t - kz) \tag{1.37}$$

Integrating Eq. (1.37) with respect to z

$$H_y = \frac{\varepsilon\omega E_{x0}}{k}cos(\omega t - kz) + D \tag{1.38}$$

where D is a constant of integration and could depend on t. Comparing Eqs. (1.35) and (1.38), we see that D is zero and using Eq. (1.36) we find

$$\frac{E_{x0}}{H_{y0}} = \frac{1}{\varepsilon\upsilon} = \eta \tag{1.39}$$

where η is the intrinsic impedance of the dielectric medium. For free space, $\eta = 376.47$ 0hms. Note that E_x and H_y are independent of x and y. In other words, at time t, the phase $\omega t - kz$ is constant in a transverse plane described by z = constant and therefore, they are called plane waves.

1.3.2 Complex Notation

It is often convenient to use complex notation for electric and magnetic fields in the following forms:

$$\tilde{E}_x = E_{x0}e^{i(\omega t - kz)} \text{ or } \tilde{E}_x = E_{x0}e^{-i(\omega t - k\ )} \tag{1.40}$$

And

$$\tilde{H}_y = H_{y0}e^{i(\omega t - k\ )} \text{ or } \tilde{H}_y = H_{y0}e^{-i(\omega t - kz)} \tag{1.41}$$

This is known as an analytic representation. The actual electric and magnetic fields can be obtained by

$$E_x = Re[\tilde{E}_x] = E_{x0}cos(\omega t - kz) \tag{1.42}$$

And

$$H_y = Re\left[\tilde{H}_y\right] = H_{y0}cos(\omega t - kz) \tag{1.43}$$

In reality, the electric and magnetic fields are not complex, but we represent them in the complex forms of Eqs. (1.40) and (1.41) with the understanding that the real parts of the complex fields correspond to the actual electric and magnetic fields. This representation leads to mathematical simplifications. For example, differentiation of a complex exponential function is the complex exponential function multiplied by some constant. In the analytic representation, superposition of two electromagnetic fields corresponds to addition of two complex fields. However, care should be

exercised when we take the product of two electromagnetic fields as encountered in nonlinear optics. For example, consider the product of two electrical fields given by

$$E_{xn} = A_n cos(\omega_n t - k_n z),\ n = 1,2 \tag{1.44}$$

$$E_{x1}E_{x2} = \frac{A_1A_2}{2} cos[(\omega_1+\omega_2)t - (k_1+k_2)z] + cos[(\omega_1-\omega_2)t - (k_1-k_2)z] \tag{1.45}$$

The product of the electromagnetic fields in the complex forms is

$$\tilde{E}_{x1}\tilde{E}_{x2} = A_1A_2 exp[i(\omega_1+\omega_2)t - i(k_1+k_2)z] \tag{1.46}$$

If we take the real part of Eq. (1.46), we find

$$Re[\tilde{E}_{x1}\tilde{E}_{x2}] = A_1A_2 cos[(\omega_1+\omega_2)t - (k_1+k_2)z] \neq E_{x1}E_{x2} \tag{1.47}$$

In this case, we should use the real form of electromagnetic fields. In the rest of this chapter we sometimes omit "˜" and use $E_x(H_y)$ to represent a complex electric (magnetic) field with the understanding that the real part is the actual field.

1.4 Power Flow and Poynting Vector

Consider an electromagnetic wave propagating in a region *V* with the cross-sectional area *A* as shown in Fig. 1.1.

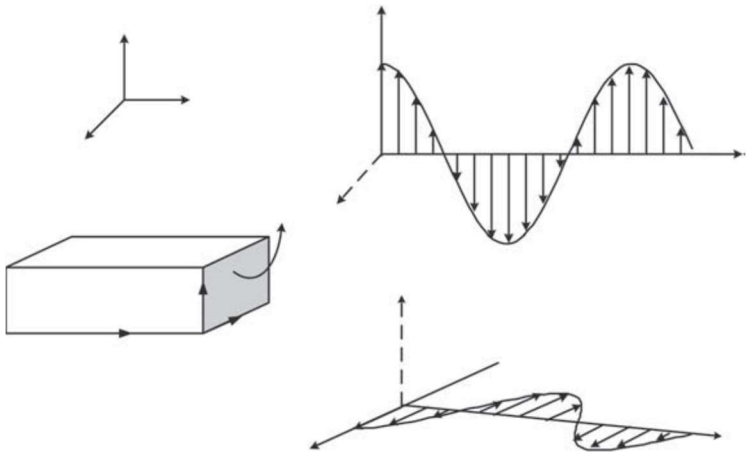

Figure 1.1 Electromagnetic wave propagation in a volume *V* with cross-sectional area *A*.

The propagation of a plane electromagnetic wave in the source-free region is governed by Eqs. (1.11) and (1.8)

$$\varepsilon \frac{\partial E_x}{\partial t} = -\frac{\partial H_y}{\partial z} \tag{1.48}$$

$$\mu \frac{\partial H_y}{\partial t} = -\frac{\partial E_x}{\partial z} \tag{1.49}$$

Multiplying Eq. (1.48) by E_x and noting that

$$\frac{\partial {E_x}^2}{\partial t} = 2E_x \frac{\partial E_x}{\partial t} \tag{1.50}$$

we obtain

$$\frac{\varepsilon}{2} \frac{\partial {E_x}^2}{\partial t} = -E_x \frac{\partial H_y}{\partial z} \tag{1.51}$$

Similarly, multiplying Eq. (1.49) by *Hy*, we have

$$\frac{\mu}{2} \frac{\partial {H_y}^2}{\partial t} = -H_y \frac{\partial E_x}{\partial z} \tag{1.52}$$

Adding Eqs. (1.52) and (1.51) and integrating over the volume *V*, we obtain

$$\frac{\partial}{\partial t} \int_V \left[\frac{\varepsilon {E_x}^2}{2} + \frac{\mu {H_y}^2}{2} \right] dV = -A \int_0^L \left[E_x \frac{\partial H_y}{\partial z} + H_y \frac{\partial E_x}{\partial z} \right] dz \tag{1.53}$$

On the right-hand side of Eq. (1.53), integration over the transverse plane yields the area *A* since E_x and H_y are functions of *z* only. Eq. (1.53) can be rewritten as

$$\frac{\partial}{\partial t} \int_V \left[\frac{\varepsilon {E_x}^2}{2} + \frac{\mu {H_y}^2}{2} \right] dV = -A \int_0^L \frac{\partial}{\partial z} \left[E_x H_y \right] dz = -A E_x H_y \Big|_0^L \tag{1.54}$$

The terms $\varepsilon {E_x}^2/2$ and $\mu {H_y}^2/2$ represent the *energy densities* of the electric field and the magnetic field, respectively. The left-hand side of Eq. (1.54) can be

interpreted as the power crossing the area A and therefore, $E_x H_y$ is the power per unit area or the *power density* measured in watts per square meter (W/m^2). We define a Poynting vector P as

$$P = E \times H \tag{1.55}$$

The z-component of the Poynting vector is

$$P_Z = E_x H_y \tag{1.56}$$

The direction of the Poynting vector is normal to both **E** and **H**, and is in fact the direction of power flow.
In Eq. (1.54), integrating the energy density over volume leads to energy $\mathcal{E}$ and, therefore, it can be rewritten as

$$\frac{1}{A}\frac{d\mathcal{E}}{dt} = P_Z(0) - P_Z(L) \tag{1.57}$$

The left-hand side of (1.57) represents the rate of change of energy per unit area and therefore, P_Z has the dimension of power per unit area or power density. For light waves, the power density is also known as the *optical intensity*. Eq. (1.57) states that the difference in the power entering the cross-section A and the power leaving the cross-section A is equal to the rate of change of energy in the volume V. The plane-wave solutions for E_x and H_y are given by Eqs. (1.32) and (1.35)

$$E_x = E_{x0} cos(\omega t - kz) \tag{1.58}$$

$$H_y = H_{y0} cos(\omega t - kz) \tag{1.59}$$

$$P_Z = \frac{E_{x0}^2}{\eta} cos^2(\omega t - kz) \tag{1.60}$$

The average power density may be found by integrating it over one cycle and dividing by the period $T = 1/f$

$$P_z^{av} = \frac{1}{T}\frac{E_{x0}^2}{\eta}\int_0^T cos^2(\omega t - kz)dt \tag{1.61}$$

$$P_z^{av} = \frac{1}{T}\frac{E_{x0}^2}{\eta}\int_0^T \frac{1+co\ [2(\omega t-k\ )]}{2}dt \tag{1.62}$$

$$P_z^{av} = \frac{E_{x0}^2}{\eta} \tag{1.63}$$

The integral of the cosine function over one period is zero and, therefore, the second term of Eq. (1.63) does not contribute after the integration. The average power density P_z^{av} is proportional to the square of the electric field amplitude. Using complex notation, Eq. (1.56) can be written as

$$P_Z = Re[\tilde{E}_x]Re\left[\tilde{H}_y\right] \tag{1.64}$$

$$P_Z = \frac{1}{\eta}Re[\tilde{E}_x]Re[\tilde{E}_x] = \frac{1}{\eta}\left[\frac{\tilde{E}_x+\tilde{E}_x^*}{2}\right]\left[\frac{\tilde{E}_x+\tilde{E}_x^*}{2}\right] \tag{1.65}$$

The right-hand side of Eq. (1.65) contains product terms such as $\tilde{E}_x^2$ and $\tilde{E}_x^{*2}$. The average of E_x^2 and E_x^{*2} over the period T is zero, since they are sinusoids with no d.c. component. Therefore, the average power density is given by

$$P_z^{av} = \frac{1}{2\eta T}\int_0^T \left|\tilde{E}_x\right|^2 dt = \frac{|\tilde{E}_x|^2}{2\eta} \tag{1.66}$$

Since $\left|\tilde{E}_x\right|^2$ is a constant for the plane wave. Thus, we see that, in complex notation, the average power density is proportional to the absolute square of the field amplitude.

Example 1.1

Two monochromatic waves are superposed to obtain

$$\tilde{E}_x = A_1 exp[i(\omega_1 t - k_1 z)] + A_2 exp[i(\omega_2 t - k_2 z)] \tag{1.67}$$

Find the average power density of the combined wave.

Solution:

From Eq. (1.66), we have

$$P_z^{av} = \frac{1}{2\eta T}\int_0^T \left|\tilde{E}_x\right|^2 dt$$

$$P_z^{av} = \frac{1}{2\eta T}\left\{T|A_1|^2 + T|A_2|^2 + A_1A_2^* \int_0^T exp[i(\omega_1 - \omega_2)t - i(k_1 - k_2)z] + A_2A_1^* \int_0^T exp[-i(\omega_1 - \omega_2)t + i(k_1 - k_2)z]\right\} dt \quad (1.68)$$

Since integrals of sinusoids over the period *T* are zero, the last two terms in Eq. (1.68) do not contribute, which leads to

$$P_z^{av} = \frac{|A_1|^2 + |A_2|^2}{2\eta} \quad (1.69)$$

Thus, the average power density is the sum of absolute squares of the amplitudes of monochromatic waves.

1.5 3-Dimensional Wave Equation

From Maxwell's equations, the following wave equation could be derived:

$$\frac{\partial^2\psi}{\partial x^2} + \frac{\partial^2\psi}{\partial y^2} + \frac{\partial^2\psi}{\partial z^2} - \frac{1}{v^2}\frac{\partial^2\psi}{\partial t^2} = 0 \quad (1.70)$$

where ψ is any one of the components *Ex*, *Ey*, *Ez*, *Hx*, *Hy*, *Hz*. As before, let us try a trial solution of the form

$$\psi = f\left(t - \alpha_x x - \alpha_y y - \alpha_z z\right) \quad (1.71)$$

We find that

$$\alpha_x^2 + \alpha_y^2 + \alpha_z^2 = \frac{1}{v^2} \quad (1.72)$$

If we choose the function to be a cosine function, we obtain a 3-dimensional plane wave described by

$$\psi = \psi_0 cos\left[\omega\left(t - \alpha_x x - \alpha_y y - \alpha_z z\right)\right] \tag{1.73}$$

$$\psi = \psi_0 \cos\left(\omega t - k_x x - k_y y - k_z z\right) \tag{1.74}$$

Where $k_r = \omega\alpha_r, r = x, y, z$. Define a vector $\boldsymbol{k} = k_x\boldsymbol{x} + k_y\boldsymbol{y} + k_z\boldsymbol{z}$. $\boldsymbol{k}$ is known as a *wave vector*. Eq. (1.72) becomes

$$\frac{\omega^2}{k^2} = v^2 \text{ or } \frac{\omega}{k} = \pm v \tag{1.75}$$

where *k* is the magnitude of the vector $\boldsymbol{k}$

$$k = \sqrt{k_x^2 + k_y^2 + k_z^2} \tag{1.76}$$

k is also known as the *wavenumber*. The angular frequency *ω* is determined by the light source, such as a laser or light-emitting diode (LED). In a linear medium, the frequency of the launched electromagnetic wave cannot be changed. The frequency of the plane wave propagating in a medium of refractive index *n* is the same as that of the source, although the wavelength in the medium decreases by a factor *n*. For given angular frequency *ω*, the wavenumber in a medium of refractive index *n* can be determined by

$$k = \frac{\omega}{v} = \frac{\omega n}{c} = \frac{2\pi n}{\lambda_0} \tag{1.77}$$

Where $\lambda_0 = c/f$ is the free-space wavelength. For free space, *n* = 1 and the wavenumber is

$$k_0 = \frac{2\pi}{\lambda_0} \tag{1.78}$$

The wavelength λ_m in a medium of refractive index *n* can be defined by

$$k = \frac{2\pi}{\lambda_m} \tag{1.79}$$

Comparing (77) and (79), it follows that

$$\lambda_m = \frac{\lambda_0}{n} \tag{1.80}$$

Example 1.2

Consider a plane wave propagating in the *x*–*z* plane making an angle of 30∘ with the *z*-axis. This plane wave may be described by

$$\psi = \psi_0 \cos\left(\omega t - k_x x - k_z z\right) \tag{1.81}$$

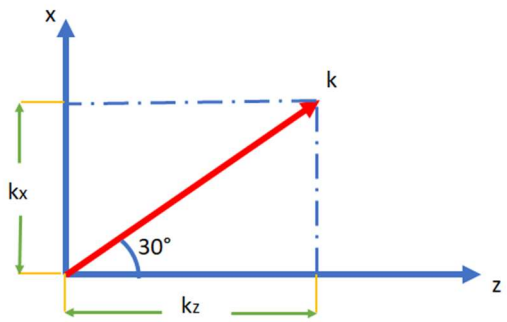

Figure 1.2 A plane wave propagates at angle 30° with the *z*-axis.

The wave vector $\boldsymbol{k} = k_x \boldsymbol{x} + k_y \boldsymbol{y}$. From Fig. 1.15, $k_x = kcos60^\circ = k/2$and $k_z = kcos30^\circ = k\sqrt{3/2}$. Eq. (1.81) may be written as

$$\psi = \psi_0 \cos\left[\omega t - k\left(\frac{1}{2}x + \frac{\sqrt{3}}{2}z\right)\right] \tag{1.82}$$

Chapter II
Reflection and Refraction

Introduction

Reflection and refraction occur when light enters into a new medium with a different refractive index. Consider a ray incident on the mirror MM', as shown in Fig. 2.1. According to the law of reflection, the angle of reflection ϕ_r is equal to the angle of incidence ϕ_i

$$\phi_i = \phi_r$$

The above result can be proved from Maxwell's equations with appropriate boundary conditions. Instead, let us use *Fermat's principle* to prove it. There are an infinite number of paths to go from point A to point B after striking the mirror. Fermat's principle can be stated loosely as follows: out of the infinite number of paths to go from point A to point B, light chooses the path that takes the shortest transit time. In Fig. 2.2, light could choose $AC'B$, $AC''B$, $AC'''B$, or any other path. But it chooses the path AC′B, for which $\phi_i = \phi_r$. Draw the line $M'B' = BM'$ so that $BC' = C'B'$, $BC'' = C''B'$, and so on. If AC′B′ is a straight line, it would be the shortest of all the paths connecting A and B'. Since $AC'B$ $(= AC'B')$, it would be the shortest path to go from A to B after striking the mirror and therefore, according to Fermat's principle, light chooses the path $AC'B$ which takes the shortest time. To prove that $\phi_i = \phi_r$, consider the point C'. Adding up all the angles at C', we find

$$\phi_i + \phi_r + 2(\pi/2 - \phi_r) = 2\pi \qquad (2.1)$$

Or

$$\phi_i = \phi_r \qquad (2.2)$$

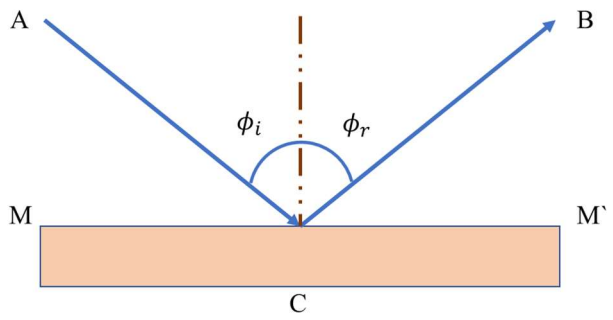

Figure 2.1 Reflection of a light wave incident on a mirror.

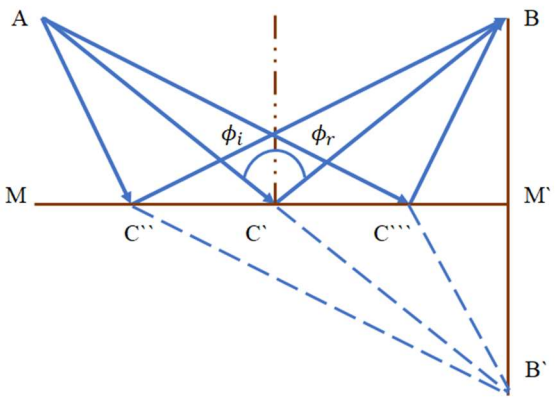

Figure 2.2 Illustration of Fermat's principle.

2.1 Refraction

In a medium with constant refractive index, light travels in a straight line. But as the light travels from a rarer medium to a denser medium, it bends toward the normal to the interface, as shown in Fig. 2.3. This phenomenon is called *refraction*, and it can be explained using Fermat's principle. Since the speeds of light in two media are different, the path which takes the shortest time to reach B from A may not be a straight-line AB. Feynmann *et al*. give the following analogy: suppose there is a little girl drowning in the sea at point B and screaming for help as illustrated in Fig. 2.4. You are at point A on the land. Obviously, the paths AC_2B and AC_3B take a longer time. You could choose the straight-line path AC_1B. But since running takes less time than swimming, it is advantageous to travel a slightly longer distance on land than sea. Therefore, the path AC_0B would take a shorter time than AC_1B. Similarly, in the case of light propagating from a rare medium to a dense medium (Fig. 2.5), light travels faster in the rare medium and therefore, the path AC_0B may take a shorter time than AC_1B. This explains why light bends toward the normal. To obtain a relation between the angle of incidence ϕ_1 and the angle of refraction ϕ_2, let us consider the time taken by light to go from A to B via several paths:

$$t_x = \frac{n_1 AC_x}{c} + \frac{n_2 C_x B}{c}, \quad x = 0,1,2 \ldots \ldots \tag{2.3}$$

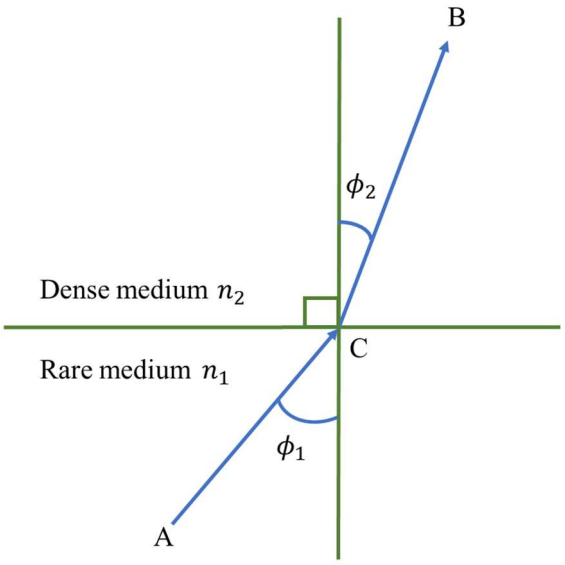

Figure 2.3 Refraction of a plane wave incident at the interface of two dielectrics.

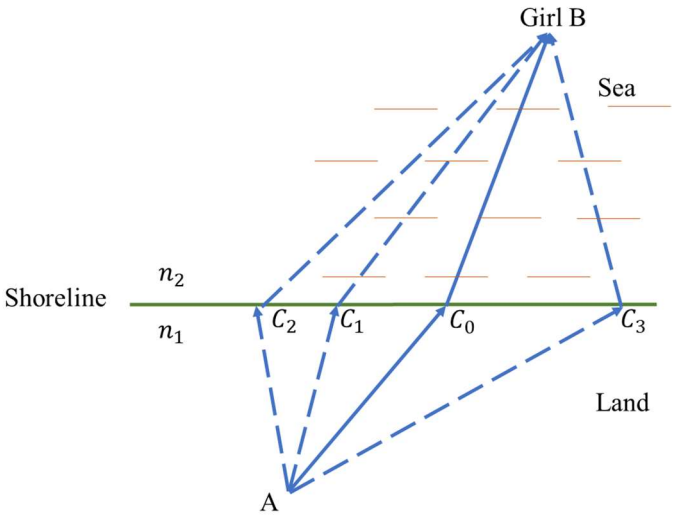

Figure 2.4 Different paths to connect A and B.

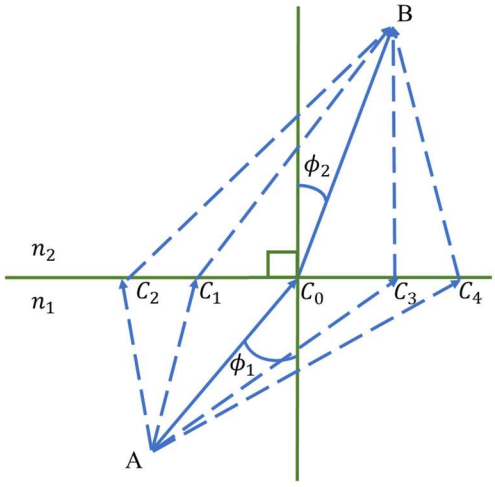

Figure 2.5 Illustration of Fermat's principle for the case of refraction.

From Fig. 2.6, we have

$$AD = x,\ C_xD = y,\ AC_x = \sqrt{x^2 + y^2} \tag{2.4}$$

$$BE = AF - x,\ BC_x = \sqrt{(AF - x)^2 + BG^2} \tag{2.5}$$

Substituting this in Eq. (2.3), we find

$$t_x = \frac{n_1\sqrt{x^2+y^2}}{c} + \frac{n_2\sqrt{(AF-x)^2+BG^2}}{c} \tag{2.6}$$

Note that AF, BG, and y are constants as x changes. Therefore, to find the path that takes the least time, we differentiate t_x with respect to x and set it to zero

$$\frac{dt_x}{dx} = \frac{n_1 x}{\sqrt{x^2+y^2}} - \frac{n_2(AF-\ )}{\sqrt{(AF-x)^2+BG^2}} = 0 \tag{2.7}$$

From Fig. 2.6, we have

$$\frac{x}{\sqrt{x^2+y^2}} = sin\phi_1, \frac{AF-x}{\sqrt{(AF-x)^2+BG^2}} = sin\phi_2 \tag{2.8}$$

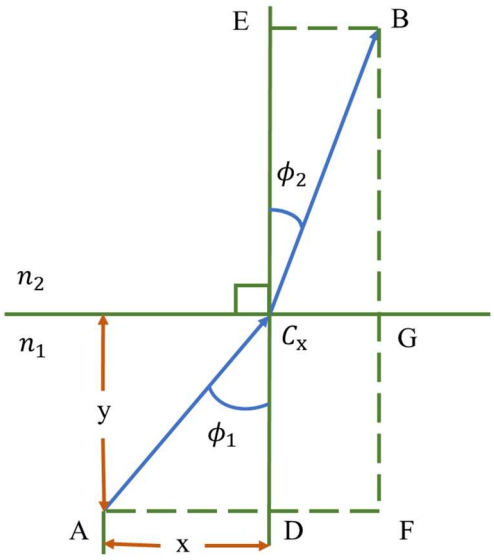

Figure 2.6 Refraction of a light wave.

Therefore, Eq. (2.7) becomes

$$n_1 sin\phi_1 = n_2 sin\phi_2 \tag{2.9}$$

This is called *Snell's law*. If $n_2 > n_1$, $sin\phi_1 > sin\phi_2$and $\phi_1 > \phi_2$. This explains why light bends toward the
normal in a denser medium, as shown in Fig. 2.6.
When $n_1 > n_2$, from Eq. (2.9), we have $\phi_2 > \phi_1$. As the angle of incidence ϕ_1 increases, the angle of refraction ϕ_2 increases too. For a particular angle, $\phi_1 = \phi_c$, ϕ_2 becomes $\pi/2$

$$n_1 sin\phi_c = n_2 sin\,\pi/2 \tag{2.10}$$

Or

$$sin\phi_c = n_2/n_1 \tag{2.11}$$

The angle ϕ_c is called the *critical angle*. If the angle of incidence is increased beyond the critical angle, the incident optical ray is reflected completely as shown in Fig. 2.7. This is called *total internal reflection* (TIR), and it plays an important role in the propagation of light in optical fibers.
Note that the statement that light chooses the path that takes the least time is not strictly correct. In Fig. 2.1, the time to go from A to B directly (without passing

through the mirror) is the shortest and we may wonder why light should go through the mirror. However, if we put the constraint that light has to pass through the mirror, the shortest path would be ACB and light indeed takes that path. In reality, light takes the direct path

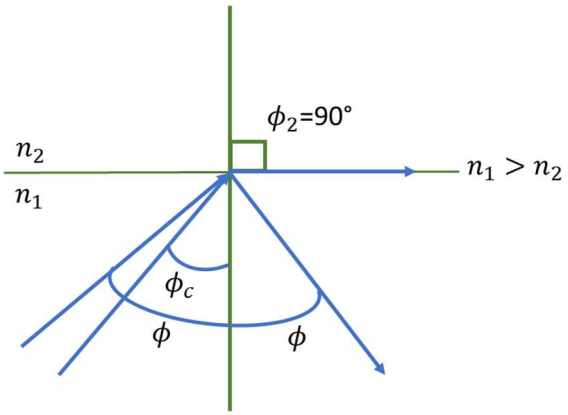

Figure 2.7 Total internal reflection when $\phi > \phi_c$.

AB as well as ACB. A more precise statement of Fermat's principle is that light chooses a path for which the transit time is an *extremum*. In fact, there could be several paths satisfying the condition of extremum and light chooses all those paths. By extremum, we mean there could be many neighboring paths and the change of time of flight with a small change in the path length is zero to first order.

Example 2.1

The critical angle for the glass–air interface is 0.7297 rad. Find the refractive index of glass.

Solution:

The refractive index of air is close to unity. From Eq. (2.11), we have

$$sin\phi_c = n_2/n_1 \tag{2.12}$$

With n_2= 1, the refractive index of glass, n_1 is

$$n_1 = 1/sin\phi_c = 1.5 \tag{2.13}$$

Example 2.2

The output of a laser operating at 190 THz is incident on a dielectric medium of refractive index 1.45. Calculate

(a) the speed of light.

(b) the wavelength in the medium.

(c) the wavenumber in the medium.

Solution:

(a) The speed of light in the medium is given by

$$v = \frac{c}{n} \tag{2.14}$$

where $c = 3 \times 10^8$ m/s, $n = 1.45$, so

$$v = \frac{3 \times 10^8 \text{ m/s}}{1.45} = 2.069 \times 10^8 \text{ m/s} \tag{2.15}$$

(b) We have
speed = frequency × wavelength

$$v = f \times \lambda_m \tag{2.16}$$

where $f = 190$ THz, $v = 2.069 \times 10^8$ m/s, so

$$\lambda_m = \frac{2.069 \times 10^8}{190 \times 10^{12}} m = 1.0889\, m \tag{2.17}$$

(c) The wavenumber in the medium is

$$k = \frac{2\pi}{\lambda_m} = \frac{2\pi}{1.0889 \times 10^{-6}} = 5.77 \times 10^6\, m^{-1} \tag{2.18}$$

Example 2.3

The output of the laser of Example 2.2 is incident on a dielectric slab with an angle of incidence $= \pi/3$, as shown in Fig. 2.8.

(a) Calculate the magnitude of the wave vector of the refracted wave.

(b) calculate the x-component and z-component of the wave vector. The other parameters are the same as in Example 2.2.

Solution:

Using Snell's law, we have

$$n_1 sin\phi_1 = n_2 sin\phi_2 \tag{2.19}$$

For air $n_1 \approx 1$, for the slab $n_2 = 1.45$, $\phi_1 = \pi/3$. So

$$\phi_2 = sin^{-1}\left\{\frac{sin(\pi/3)}{1.45}\right\} = 0.6401\, rad \tag{2.20}$$

The electric field intensity in the dielectric medium can be written as

$$E_x = Acos(\omega t - k_x x - k_z z) \tag{2.21}$$

(a) The magnitude of the wave vector is the same as the wavenumber k. It is given by

$$|k| = k = \frac{2\pi}{\lambda_m} = 5.77 \times 10^6\ m^{-1} \tag{2.22}$$

(b) The z-component of the wave vector is

$$k_z = kcos(\phi_2) = 5.77 \times 10^6 \times cos(0.6401)\ m^{-1} = 4.62 \times 10^6\ m^{-1} \tag{2.23}$$

The x-component of the wave vector is

$$k_x = ksin(\phi_2) = 5.77 \times 10^6 \times sin(0.6401)\ m^{-1} = 3.44 \times 10^6\ m^{-1} \tag{2.24}$$

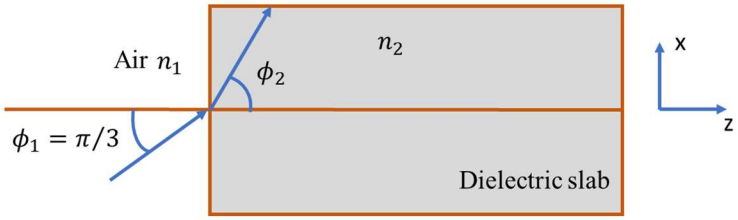

Figure 2.8 Reflection of light at air–dielectric interface.

2.2 Phase Velocity and Group Velocity

Consider the superposition of two monochromatic electromagnetic waves of frequencies $\omega_0 + \Delta\omega/2$ and $\omega_0 - \Delta\omega/2$ as shown in Fig. 2.9. Let $\Delta\omega \ll \omega_0$. The total electric field intensity can be written as

$$E = E_1 + E_2 \tag{2.25}$$

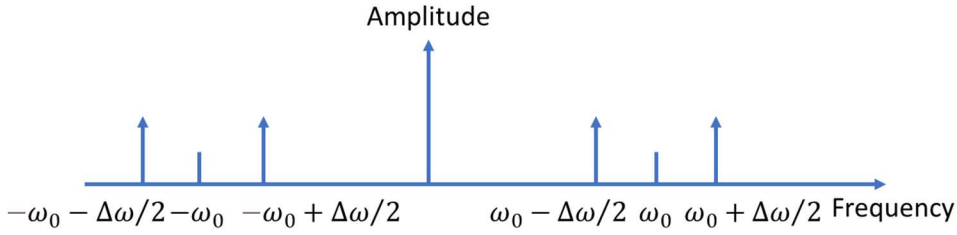

Figure 2.9 The spectrum when two monochromatic waves are superposed.

Let the electric field intensity of these waves be

$$E_1 = cos[(\omega_0 - \Delta\omega/2)t - (k - \Delta k/2)z] \tag{2.26}$$

$$E_2 = cos[(\omega_0 + \Delta\omega/2)t - (k + \Delta k/2)z] \tag{2.27}$$

Using the formula

$$\cos C + \cos D = 2cos\left(\frac{C+D}{2}\right)cos\left(\frac{C-D}{2}\right)$$

Eq. (2.25) can be written as

$$E = \underbrace{2cos(\Delta\omega t - \Delta kz)}_{field\ envelope}\ \underbrace{cos(\omega_0 t - k_0 z)}_{carrier} \tag{2.28}$$

Eq. (2.28) represents the modulation of an optical carrier of frequency ω_0 by a sinusoid of frequency $\Delta\omega$. Fig. 2.10 shows the total electric field intensity at $z = 0$. The broken line shows the field envelope and the solid line shows rapid oscillations due to the optical carrier. We have seen before that

$v_{ph} = \frac{\omega_0}{k_0}$

is the velocity of the carrier. It is called the *phase velocity*. Similarly, from Eq. (2.28), the speed with which the envelope moves are given by

$$v_g = \frac{\Delta\omega}{\Delta k} \tag{2.29}$$

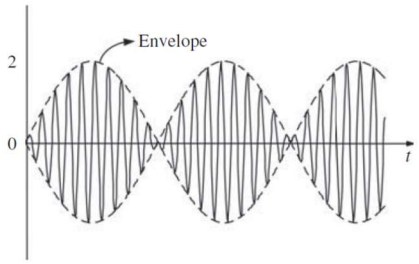

Figure 2.10 Superposition of two monochromatic electromagnetic waves. The broken lines and solid lines show the field envelope and optical carrier, respectively.

where v_g is called the *group velocity*. Even if the number of monochromatic waves traveling together is more than two, an equation similar to Eq. (2.28) can be derived. In general, the speed of the envelope (group velocity) could be different from that of the carrier. However, in free space

$v_g = v_{ph} = c$

The above result can be proved as follows. In free space, the velocity of light is independent of frequency

$$\frac{\omega_1}{k_1} = \frac{\omega_2}{k_2} = c = v_{ph} \tag{2.30}$$

Let

$$\omega_1 = \omega_0 - \frac{\Delta\omega}{2} \ , \qquad k_1 = k_0 - \frac{\Delta k}{2} \tag{2.31}$$

$$\omega_2 = \omega_0 + \frac{\Delta\omega}{2} \ , \qquad k_2 = k_0 + \frac{\Delta k}{2} \tag{2.32}$$

From Eqs. (2.31) and (2.32), we obtain

$$\frac{\omega_2 - \omega_1}{k_2 - k_1} = \frac{\Delta\omega}{\Delta k} = v_g \tag{2.33}$$

From Eq. (2.30), we have

$$\omega_1 = ck_1$$

$$\omega_2 = ck_2$$

$$\omega_1 - \omega_2 = c(k_1 - k_2) \tag{2.34}$$

Using Eqs. (2.33) and (2.34), we obtain

$$\frac{\omega_1 - \omega_2}{k_1 - k_2} = c = v_g \tag{2.35}$$

In a dielectric medium, the velocity of light v_{ph} could be different at different frequencies. In general

$$\frac{\omega_1}{k_1} \neq \frac{\omega_1}{k_2} \tag{2.36}$$

In other words, the phase velocity v_{ph} is a function of frequency

$$v_{ph} = v_{ph}(\omega) \tag{2.37}$$

$$k = \frac{\omega}{v_{ph}(\omega)} = k(\omega) \tag{2.38}$$

In the case of two sinusoidal waves, the group speed is given by Eq. (2.29)

$$v_g = \frac{\Delta\omega}{\Delta k} \tag{2.39}$$

In general, for an arbitrary cluster of waves, the group speed is defined as

$$v_g = \lim_{\Delta k \to 0} \frac{\Delta \omega}{\Delta k} = \frac{\mathrm{d}\omega}{\mathrm{d}k} \tag{2.40}$$

Sometimes it is useful to define the *inverse group speed* β_1 as

$$\beta_1 = \frac{1}{v_g} = \frac{dk}{d\omega} \tag{2.41}$$

β_1 could depend on frequency. If β_1 changes with frequency in a medium, it is called a *dispersive medium*. Optical fiber is an example of a dispersive medium, which will be discussed in detail in Chapter 2. If the refractive index changes with frequency, β_1 becomes frequency dependent. Since

$$k(\omega) = \frac{\omega n(\omega)}{c} \tag{2.42}$$

from Eq. (2.41) it follows that

$$\beta_1(\omega) = \frac{n(\omega)}{c} + \frac{\omega}{c}\frac{dn(\omega)}{d\omega} \tag{2.43}$$

Another example of a dispersive medium is a prism, in which the refractive index is different for different frequency components. Consider a white light incident on the prism, as shown in Fig. 2.11. Using Snell's law for the air–glass interface on the left, we find

$$\phi_2(\omega) = sin^{-1}\left(\frac{sin\phi_1}{n_2(\omega)}\right) \tag{2.44}$$

where $n_2(\omega)$ is the refractive index of the prism. Thus, different frequency components of a white light travel at different angles, as shown in Fig. 2.11. Because of the material dispersion of the prism, a white light is spread into a rainbow of colors.

Next, let us consider the co-propagation of electromagnetic waves of different angular frequencies in a range $[\omega_1, \omega_2]$ with the mean angular frequency ω_0 as shown in Fig. 2.12. The frequency components near the left edge travel at an inverse speed of $\beta_1(\omega_1)$. If the length of the medium is L, the frequency components corresponding to the left edge would arrive at L after a delay of

$$T_1 = \frac{L}{v_g(\omega_1)} = \beta_1(\omega_1)L$$

Similarly, the frequency components corresponding to the right edge would arrive at L after a delay of

$$T_2 = \beta_1(\omega_2)L$$

The delay between the left-edge and the right-edge frequency components is

$$\Delta T = |T_1 - T_2| = |\beta_1(\omega_1) - \beta_1(\omega_2)| \tag{2.45}$$

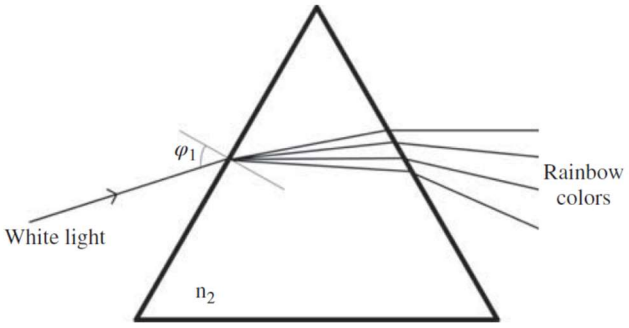

Figure 2.11 Decomposition of white light into its constituent colors.

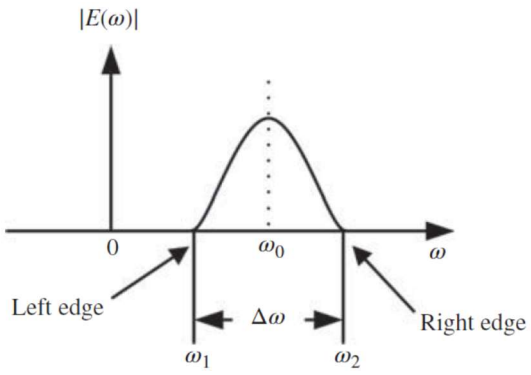

Figure 2.12 The spectrum of an electromagnetic wave.

Differentiating Eq. (2.41), we obtain

$$\frac{d\beta_1}{d\omega} = \frac{d^2k}{d\omega^2} \equiv \beta_2 \tag{2.46}$$

β_2 is called the *group velocity dispersion* parameter. When $\beta_2 > 0$, the medium is said to exhibit a *normal dispersion*. In the normal-dispersion regime, low-frequency (red-shifted) components travel faster than high-frequency (blue-shifted) components. If $\beta_2 < 0$, the opposite occurs and the medium is said to exhibit an *anomalous dispersion*. Any medium with $\beta_2 = 0$ is non-dispersive. Since

$$\frac{d\beta_1}{d\omega} = \lim_{\Delta\omega \to 0} \frac{\beta_1(\omega_1) - \beta_1(\omega_2)}{\omega_1 - \omega_2} = \beta_2 \tag{2.47}$$

And

$$\beta_1(\omega_1) - \beta_1(\omega_2) \simeq \beta_2 \Delta\omega \tag{2.48}$$

using Eq. (2.48) in Eq. (2.45), we obtain

$$\Delta T = L|\beta_2|\Delta\omega \tag{2.49}$$

In free space, β_1 is independent of frequency, $\beta_2 = 0$, and, therefore, the delay between left- and right-edge components is zero. This means that the pulse duration at the input ($z = 0$) and output ($z = L$) would be the same. However, in a dispersive medium such as optical fiber, the frequency components near ω_1 could arrive earlier (or later) than those near ω_2, leading to pulse broadening.

Example 2.4

An optical signal of bandwidth 100 GHz is transmitted over a dispersive medium with $\beta_2 = 10$ ps^2/km. The delay between minimum and maximum frequency components is found to be 3.14 ps. Find the length of the medium.

Solution:

$\Delta\omega = 2\pi 100\, Grad/s, \quad \Delta T = 3.14ps, \ \beta_2 = 10p\, s^2/km$

(2.50)

Substituting Eq. (2.50) in Eq. (2.49), we find $L = 500$ m.

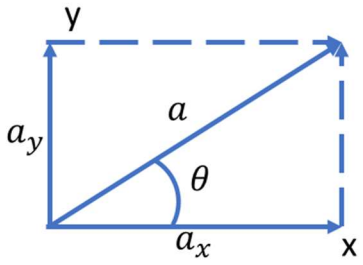

Figure 2.13 The x- and y-polarization components of a plane wave. The magnitude is $|a| = \sqrt{a_x^2 + a_y^2}$ and the angle is $\theta = \tan^{-1}(a_y/a_x)$

2.3 Polarization of Light

So far, we have assumed that the electric and magnetic fields of a plane wave are along the x-and y-directions, respectively. In general, an electric field can be in any direction in the x–y plane. This plane wave propagates in the z-direction. The electric field intensity can be written as

$$\boldsymbol{E} = A_x\boldsymbol{x} + A_y\boldsymbol{y} \tag{2.51}$$

$$A_x = a_x exp[i(\omega t - kz) + i\phi_x] \tag{2.52}$$

$$A_y = a_y exp\left[i(\omega t - kz) + i\phi_y\right] \tag{2.53}$$

where a_x and a_y are amplitudes of the x- and y-polarization components, respectively, and ϕ_x and ϕ_y are the corresponding phases. Using Eqs. (2.52) and (2.53), Eq. (2.51) can be written as

$$E = \boldsymbol{a}\, exp[i(\omega t - kz) + i\phi_x] \tag{2.54}$$

$$\boldsymbol{a} = a_x \boldsymbol{x} + a_y exp(i\Delta\phi)\boldsymbol{y} \tag{2.55}$$

where $\Delta\phi = \phi_y - \phi_x$. Here, $\boldsymbol{a}$ is the complex field envelope vector. If one of the polarization components vanishes ($a_y = 0$, for example), the light is said to be *linearly polarized* in the direction of the other polarization component (the *x*-direction). If $\Delta\phi = 0$ or π, the light wave is also linearly polarized. This is because the magnitude of $\boldsymbol{a}$ in this case is $a_x^2 + a_y^2$ and the direction of $\boldsymbol{a}$ is determined by $\theta = \pm \tan^{-1}(a_y/a_x)$ with respect to the *x*-axis, as shown in Fig. 2.13. The light wave is linearly polarized at an angle θ with respect to the *x*-axis. A plane wave of angular frequency ω is characterized completely by the complex field envelope vector $\boldsymbol{a}$. It can also be written in the form of a column matrix, known as the *Jones vector*:

$$a = \begin{bmatrix} a_x \\ a_y exp(i\Delta\emptyset) \end{bmatrix} \tag{2.56}$$

The above form will be used for the description of polarization mode dispersion in optical fibers.

Chapter III
Fiber Characteristic

3.1. Introduction

In its simplest form, an optical fiber consists of a central glass core surrounded by a cladding layer whose refractive index n_c is slightly lower than the core index n_1. Such fibers are generally referred to as *step-index fibers* to distinguish them from *graded-index fibers* in which the refractive index of the core decreases gradually from center to core boundary. Figure 3.1 shows schematically the cross-section and refractive-index profile of a step-index fiber. Two parameters that characterize an optical fiber are the relative core–cladding index difference:

$$\Delta = \frac{n_1 - n_c}{n_1} \tag{3.1}$$

and the so-called V parameter defined as

$$V = k_0 a \sqrt{(n_1^2 - n_c^2)} \tag{3.2}$$

Where $k_0 = 2\pi/\lambda$, a is the core radius, and λ is the wavelength of light.
The V parameter determines the number of modes supported by the fiber. Where it is shown that a step-index fiber supports a single-mode if $V < 2.405$. Optical fibers designed to satisfy this condition are

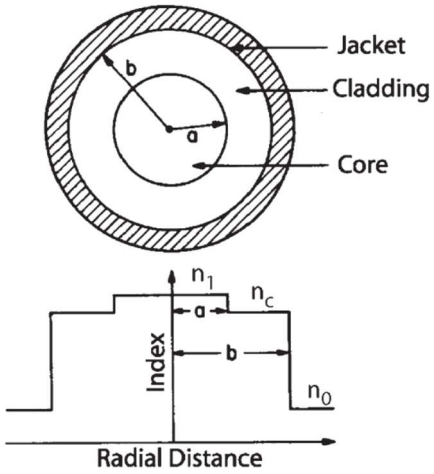

Figure 3.1 Schematic illustration of the cross-section and the refractive-index profile of a step-index fiber.

called single-mode fibers. The main difference between the single-mode and multimode fiber is the core size. The core radius a is typically 25 μm for multimode fibers. However, single-mode fibers with $\Delta \approx 0.003$ require a to be <5 μm. The numerical value of the outer radius b is less critical as long as it is large enough to confine the fiber modes entirely. A standard value of $b = 62.5$ μm is commonly used for both single-mode and multimode fibers. Since nonlinear effects are mostly studied using single-mode fibers, the term optical fiber in this text refers to single-mode fibers (unless noted otherwise).

3.2. Advantages of Optical Fiber

There are several advantages of optical communication systems over electronic and microwave communication systems. The main advantages are summarized below.

High Bandwidth: The information carrying capacity of a communication system is directly proportional to the carrier frequency of the transmitted signals. The optical carrier frequency is much greater than the radio waves and microwaves. Generally, optical fiber operates in the range of 1013–1015 Hz. This frequency band has higher transmission bandwidth than the microwave
band, and the data rate ~1 Tb/s. Further increase in data rate can be achieved by danced WDM techniques.

Low Transmission Loss: Due to the implementation of ultra-low loss fibers, dispersion shifted fiber and erbium doped silica fibers as optical amplifiers, one can design almost lossless transmission systems. The most modern optical communication systems have transmission loss of 0.002 dB/km. By using erbium doped silica fibers over a short length in the transmission path, one can achieve optical amplification with negligible distortion. This leads to the increase in repeater spacing >100 km.

Dielectric Waveguide: Optical fibers are mainly produced from silica, which is electrical insulators. Since optical signals in fibers are free from electromagnetic interference and crosstalk, many fibers may be accommodated in single optical cable. Optical fibers are also suitable in explosive environments.

Signal Security: The information security in optical communication is very high because the transmitted signal through the fibers does not radiate. The trapping of optical information from the fibers is practically impossible.

Size and Weight: Optical fibers are developed with small diameter, and they are flexible, compact and lightweight. The fiber cables can be bent or twisted without

any damage of the individual fibers. Therefore, the storage, handling and installation of fiber cables are easy.

3.3. Fiber Losses

Signal attenuation or loss in optical fiber is caused by a number of processes like absorption, scattering, bending, etc. Signal loss or attenuation depends on the wavelength of light that propagates through the fiber. For a particular wavelength, if P_0 is the transmitted optical power at the input of a fiber of length L and P_T is the received power at the other end of the fiber, then according to Beer's law we get

$$P_T = P_0 exp(-\alpha L) \tag{3.3}$$

where the *attenuation constant* α is a measure of total fiber losses from all sources. It is customary to express α in units of dB/km using the relation

$$\alpha_{dB} = -\frac{10}{L} log\left(\frac{P_T}{P_0}\right) = 4.343\alpha \tag{3.4}$$

where Eq. (3.4) was used to relate α_{dB} and α.

As one may expect, fiber losses depend on the wavelength of light. Figure 3.2 shows the loss spectrum of a silica fiber made by the MCVD process. This fiber exhibits a minimum loss of about 0.2 dB/km near 1.55 μm. Losses are considerably higher at shorter wavelengths, reaching a level of a few dB/km in the visible region.

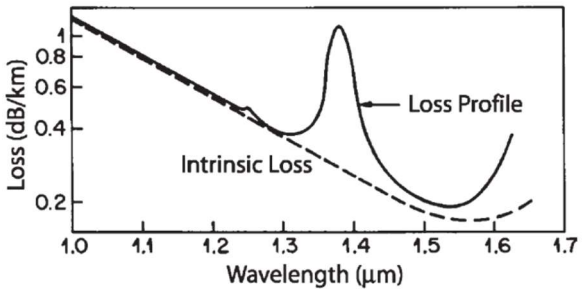

Figure 3.2 Measured loss spectrum of a single-mode silica fiber. Dashed curve shows the contribution resulting from Rayleigh scattering.

Note, however, that even a 10-dB/km loss corresponds to an attenuation constant of only $\alpha \approx 2 \times 10^{-5}$ cm^{-1}, an incredibly low value compared to that of most other materials. Several factors contribute to the loss spectrum of Figure 3.2, with material absorption and *Rayleigh scattering* contributing dominantly. Silica glass has

electronic resonances in the ultraviolet region, and vibrational resonances in the far-infrared region beyond 2 μm, but it absorbs little light in the wavelength region extending from 0.5 to 2 μm. However, even a relatively small number of impurities can lead to significant absorption in that wavelength window. From a practical point of view, the most important impurity affecting fiber loss is the OH ion, which has a fundamental vibrational absorption peak at ≈ 2.73 μm. The overtones of this OH-absorption peak are responsible for the dominant peak seen in Figure 3.2 near 1.4 μm and a smaller peak near 1.23 μm. Special precautions are taken during the fiber-fabrication process to ensure an OH-ion level of less than one part in one hundred million. In state of- the-art fibers, the peak near 1.4 μm can be reduced to below the 0.5-dB level. It virtually disappears in the so-called "dry" fibers. Such fibers with low losses in the entire 1.3–1.6 μm spectral region are useful for fiber-optic communications and were available commercially by the year 2000.

Rayleigh scattering is a fundamental loss mechanism arising from density fluctuations frozen into the fused silica during manufacture. Resulting local fluctuations in the refractive index scatter light in all directions. The Rayleigh-scattering loss varies as λ^{-4} and is dominant at short wavelengths. As this loss is intrinsic to the fiber, it sets the ultimate limit on fiber loss. The intrinsic loss level (shown by a dashed line in Figure 3.2) is estimated to be (dB/km)

$$\alpha_R = C_R/\lambda^4 \tag{3.5}$$

where the constant C_R is in the range 0.7–0.9 dB/(km μm^4) depending on the constituents of the fiber core. As α_R is in the range of 0.12–0.15 dB/km near λ = 1.55 μm, losses in silica fibers are dominated by Rayleigh scattering. In some glasses, α_R can be reduced to a level near 0.05 dB/km. Such glasses may be useful for fabricating ultralow-loss fibers. Among other factors that may contribute to losses are bending of the fiber and scattering of light at the core–cladding interface. Modern fibers exhibit a loss of ≈ 0.2 dB/km near 1.55 μm. Total loss of fiber cables used in optical communication systems is slightly larger because of splice and cabling losses.

3.4. Chromatic Dispersion

When an electromagnetic wave interacts with the bound electrons of a dielectric, the medium response, in general, depends on the optical frequency ω. This property,

referred to as chromatic dispersion, manifests through the frequency dependence of the refractive index $n(\omega)$. On a fundamental level, the origin of chromatic dispersion is related to the characteristic resonance frequencies at which the medium absorbs the electromagnetic radiation through oscillations of bound electrons. Far from the medium resonances, the refractive index is well approximated by the *Sellmeier equation*

$$n^2(\omega) = 1 + \sum_{j=1}^{m} \frac{B_j \omega_j^2}{\omega_j^2 - \omega^2} \tag{3.6}$$

where ω_j is the resonance frequency and B_j is the strength of j_{th} resonance. The sum in Eq. (3.6) extends over all material resonances that contribute to the frequency range of interest. In the case of optical fibers, the parameters B_j and ω_j are obtained experimentally by fitting the measured dispersion curves to Eq. (3.6) with $m = 3$ and they are dependant on the core constituents. For bulk-fused silica, these parameters are found to be $B_1 = 0.6961663$, $B_2 = 0.4079426$, $B_3 = 0.8974794$, $\lambda_1 = 0.0684043$ μm, $\lambda_2 = 0.1162414$ μm, and $\lambda_3 = 9.896161$ μm, where $\lambda_J = 2\pi c/\omega_j$ and c is the speed of light in a vacuum. Figure 3.3 displays how n varies with wavelength for fused silica. As seen there, n has a value of about 1.46 in the visible region, and this value decreases by 1% in the wavelength region near 1.5 μm. Fiber dispersion plays a critical role in the propagation of short optical pulses because different spectral components associated with the pulse travel at different speeds given by $c/n(\omega)$. Even when the nonlinear effects are not important, dispersion- induced pulse broadening can be detrimental for optical communication systems. In the nonlinear regime, the combination of dispersion and nonlinearity can result in a qualitatively different behavior. Mathematically, the effects of fiber dispersion are accounted for by expanding the mode-propagation

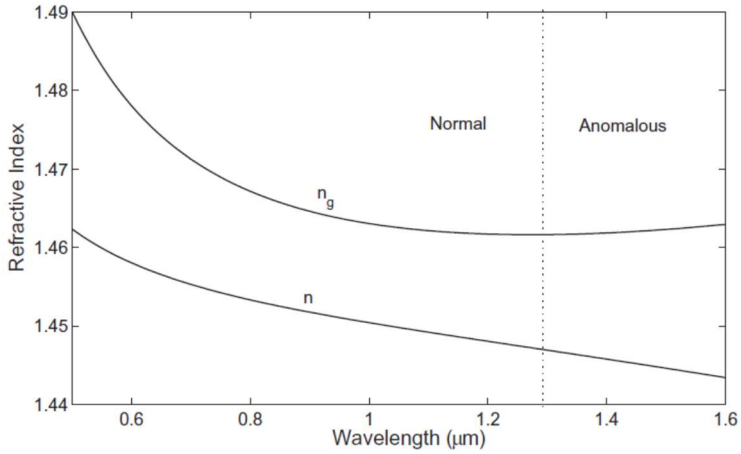

Figure 3.3 Variation of refractive index *n* and group index n_g with wavelength for fused silica.

constant β in a Taylor series about the frequency ω_0 at which the pulse spectrum is centered:

$$\beta(\omega) = n(\omega)\frac{\omega}{c} = \beta_0 + \beta_1(\omega - \omega_0) + \frac{1}{2}\beta_2(\omega - \omega_0)^2 + \cdots \quad (3.7)$$

Where

$$\beta_m = \left(\frac{d^m\beta}{d\omega^m}\right)_{\omega=\omega_0} \quad (m = 0, 1, 3 \ldots\ldots) \quad (3.8)$$

The parameters β_1 and β_2 are related to the refractive index $n(\omega)$ and its derivatives through the relations

$$\beta_1 = \frac{1}{v_g} = \frac{n_g}{c} = \frac{1}{c}\left(n + \omega\frac{dn}{d\omega}\right) \quad (3.9)$$

$$\beta_2 = \frac{1}{c}\left(2\frac{dn}{d\omega} + \omega\frac{d^2n}{d\omega^2}\right) \quad (3.10)$$

where *n*g is the group index and v_g is the group velocity. Figure 3.3 shows the group index n_g changes with wavelength for fused silica. The group velocity can be found using $v_g = c/n_g$. Physically speaking, the envelope of an optical pulse moves at the group velocity, while the parameter β_2 represents dispersion of the group velocity and is responsible for pulse broadening. This phenomenon is known as the *group velocity dispersion* (GVD), and β_2 is the GVD parameter. The dispersion parameter *D*, defined as $d\beta_1/d\lambda$, is also used in practice. It is related to β_2 and *n* as

$$D = \frac{d\beta_1}{d\lambda} = -\frac{2\pi}{\lambda^2}\beta_2 = -\frac{\lambda d^2 n}{c d\lambda^2} \tag{3.11}$$

Figure 3.4 shows how β_2 and D vary with wavelength λ for fused silica using Eqs (3.6) and (3.10). The most notable feature is that both β_2 and D vanish at a wavelength of about 1.27 μm and change sign for longer wavelengths. This wavelength is referred to as the *zero-dispersion wavelength* and is denoted as λ_D. However, the dispersive effects do not disappear completely at $\lambda = \lambda_D$. Pulse propagation near this wavelength requires the inclusion of the cubic term in Eq. (3.7). The coefficient β_3 appearing in that term is called the *third-order dispersion* (TOD) parameter. Higher order dispersive effects can distort ultrashort optical pulses both in the linear and nonlinear regimes. Their inclusion is necessary for ultrashort optical pulses, or when the input wavelength λ approaches λ_D to within a few nanometers. The curves shown in Figures 3.3 and 3.4 are for bulk-fused silica. The dispersive behavior of actual glass fibers deviates from that shown in these figures for the following two reasons. First, the fiber core may have small amounts of dopants such as GeO_2 and P_2O_5. Equation (3.6) in that case should be used with parameters appropriate to the number of doping levels. Second, because of dielectric waveguiding, the effective mode index is slightly lower than the material index $n(\omega)$ of the core, reduction itself being ω dependent.

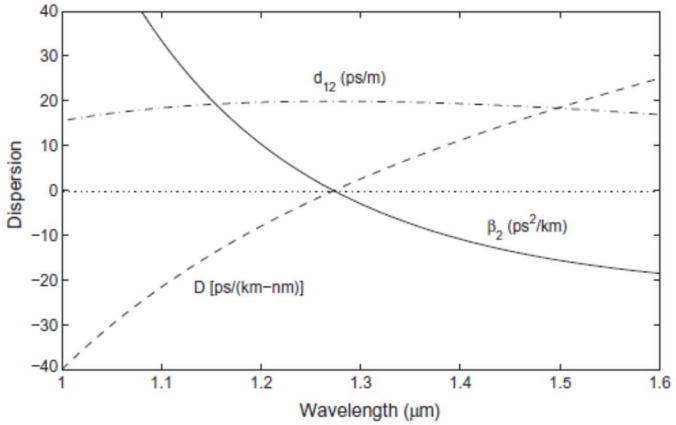

Figure 3.4 Variation of β_2, D, and d_{12} with the wavelength for fused silica. Both β_2 and D vanish at the zero-dispersion wavelength occurring near 1.27 μm.

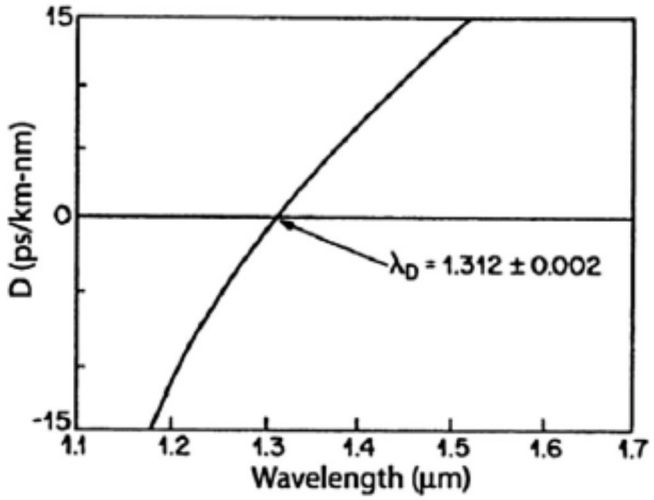

Figure 3.5 Measured variation of the dispersion parameter *D* with the wavelength for a single-mode fiber.

This results in a waveguide contribution that must be added to the material contribution to obtain the total dispersion. Generally, the waveguide contribution to β_2 is relatively small except near the zero-dispersion wavelength λ_D where the two become comparable. The main effect of the waveguide contribution is to shift λ_D slightly toward longer wavelengths; $\lambda_D \approx 1.31$ μm for standard fibers. Figure 3.5 shows the measured total dispersion of a single-mode fiber. The quantity plotted is the dispersion parameter *D* related to β_2 by the relationship given in Eq. (3.11). An interesting feature of the waveguide dispersion is that its contribution to *D* (or β_2) depends on fiber-design parameters such as core radius *a* and core–cladding index difference _. This feature can be used to shift the zero-dispersion wavelength λD in to the vicinity of 1.55 μm where the fiber loss is at a minimum. Such *dispersion-shifted* fibers have found applications in optical communication systems. They are available commercially and are known by trade names such as True Wave (OFS), LEAF (Corning), and TeraLight (Draka), depending on at what wavelength *D* becomes zero in the 1.5 μm spectral region. The fibers in which GVD is shifted to the wavelength region beyond 1.6 μm exhibit a large positive value of β_2. They are called *dispersion compensating fibers* (DCFs). The slope of the curve in Figure 3.5 (called the *dispersion slope*) is related to the TOD parameter β_3. Fibers with reduced slope have been developed in recent years for wavelength-division-multiplexing (WDM) applications. It is possible to design *dispersion-flattened* optical fibers having low dispersion over a relatively large wavelength range of 1.3–1.6 μm. This

is achieved by using multiple cladding layers. Figure 3.6 shows the measured dispersion spectra for two such multiple-clad fibers having two (double-clad) and four (quadruple-clad) cladding layers around the core applications. For comparison, dispersion of a single-clad fiber is also shown by a dashed line. The quadruply clad fiber has low dispersion ($|D| \sim 1$ ps/km-nm) over a wide wavelength range extending from 1.25 to 1.65 μm. Waveguide dispersion can also be used to make fibers for which D varies along the fiber length. An example is provided by *dispersion-decreasing* fibers made by tapering the core diameter along the fiber length.

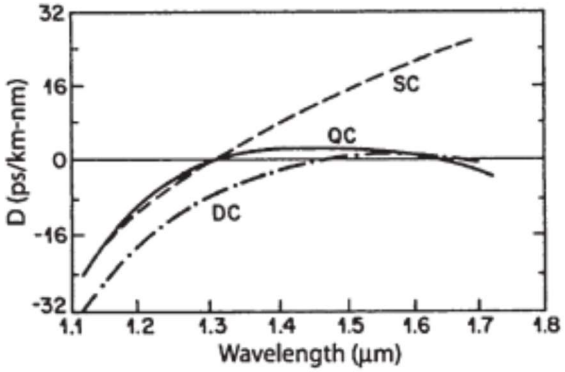

Figure 3.6 Variation of dispersion parameter D with wavelengths for three kinds of fibers. Labels SC, DC, and QC stand for single-clad, double-clad, and quadruple-clad fibers, respectively.

3.5. Nonlinear effects

Nonlinear effects in optical fibers can manifest qualitatively different behaviors depending on the sign of the GVD parameter. For wavelengths such that $\lambda < \lambda_D$, the fiber is said to exhibit *normal dispersion* as $\beta_2 > 0$ (see Figure 3.4). In the normal dispersion regime, high-frequency (blue-shifted) components of an optical pulse travel slower than low-frequency (red-shifted) components of the same pulse. By contrast, the opposite occurs in the *anomalous-dispersion* regime in which $\beta_2 < 0$. As seen in Figure 3.4, silica fibers exhibit anomalous dispersion when the light wavelength exceeds the zero-dispersion wavelength ($\lambda > \lambda_D$). The anomalous-dispersion regime is of considerable interest for the study of nonlinear effects because it is in this regime that optical fibers support solitons through a balance between the dispersive and nonlinear effects.

An important feature of chromatic dispersion is that pulses at different wavelengths propagate at different speeds inside a fiber because of a mismatch in their group velocities. This feature leads to a walk-off effect that plays an important role in the

description of the nonlinear phenomena involving two or more closely spaced optical pulses. More specifically, the nonlinear interaction between two optical pulses ceases to occur when the faster moving pulse completely walks through the slower moving pulse. This feature is governed by the *walk-off parameter* d_{12} defined as

$$d_{12} = \beta_1(\lambda_1) - \beta_1(\lambda_2) = v_g^{-1}(\lambda_1) - v_g^{-1}(\lambda_2) \tag{3.12}$$

where λ_1 and λ_2 are the center wavelengths of two pulses and β_1 at these wavelengths is evaluated using Eq. (3.9). For pulses of width T_0, one can define the walk-off length L_W by the relation

$$L_W = T_0/|d_{12}| \tag{3.13}$$

Figure 3.4 shows variation of d_{12} with λ_1 for fused silica using Eq. (3.12) with $\lambda_2 = 0.8\ \mu m$. In the normal-dispersion regime ($\beta_2 > 0$), a longer-wavelength pulse travels faster, while the opposite occurs in the anomalous-dispersion region. For example, if a pulse at $\lambda_1 = 1.3$ μm copropagates with the pulse at $\lambda_2 = 0.8\mu m$, it will separate from the shorter-wavelength pulse at a rate of about 20 ps/m. This corresponds to a walk-off length L_W of only 50 cm for $T_0 = 10$ ps. The group-velocity mismatch plays an important role for nonlinear effects involving cross-phase modulation.

3.6. Polarization-Mode Dispersion

Even a single-mode fiber is not truly single mode because it can support two degenerate modes that are polarized in two orthogonal directions.

Under ideal conditions (perfect cylindrical symmetry and a stress-free fiber), a mode excited with its polarization in the *x*-direction would not couple to the mode with the orthogonal *y*-polarization state. In real fibers, small departures from cylindrical symmetry, occurring because of random variations in the core shape along the fiber length, result in a mixing of the two polarization states by breaking the mode degeneracy. The stress-induced anisotropy can also break this degeneracy. Mathematically, the mode-propagation constant β becomes slightly different for the modes polarized in the *x*- and *y*-directions. This property is referred to as modal birefringence. The strength of modal birefringence is defined by a dimensionless parameter

$$B_m = \frac{|\beta_x - \beta_y|}{k_0} = |n_x - n_y| \tag{3.14}$$

where n_x and n_y are the modal refractive indices for the two orthogonally polarized states. For a given value of B_m, the two modes exchange their powers in a periodic fashion as they propagate inside the fiber with the period

$$L_B = \frac{2\pi}{|\beta_x - \beta_y|} = \frac{\lambda}{B_m} \tag{3.15}$$

The length L_B is called the *beat length*. The axis along which the mode index is smaller is called the *fast axis* because the group velocity is larger for light propagating in that direction. For the same reason, the axis with the larger mode index is called the *slow axis*. In standard optical fibers, *B*m is not constant along the fiber but changes randomly because of fluctuations in the core shape and anisotropic stress. As a result, light launched into the fiber with a fixed state of polarization changes its polarization in a random fashion. This change in polarization is typically harmless for continuous-wave (CW) light because most photodetectors do not respond to polarization changes of the incident light. It becomes an issue for optical communication systems when short pulses are transmitted over long lengths. If an input pulse excites both polarization components, the two components travel along the fiber at different speeds because of their different group velocities. The pulse becomes broader at the output end because group velocities change randomly in response to random changes in fiber birefringence (analogous to a random-walk problem). This phenomenon, referred to as *polarization-mode dispersion* (PMD), has been studied extensively because of its importance for long-haul lightwave systems. The extent of pulse broadening can be estimated from the time delay ΔT occurring between the two polarization components during the propagation of an optical pulse. For a fiber of length L and constant birefringence B_m, ΔT is given by

$$\Delta T = \left|\frac{L}{v_{gx}} - \frac{L}{v_{gy}}\right| = L|\beta_{1x} - \beta_{1y}| = L(\Delta\beta_1) \tag{3.16}$$

where $\Delta\beta_1$ is related to group-velocity mismatch. Eq. (3.16) cannot be used directly to estimate PMD for standard telecommunication fibers because of random changes

in birefringence occurring along the fiber. These changes tend to equalize the propagation times for the two polarization components. In fact, PMD is characterized by the root-mean-square (RMS) value of ΔT obtained after averaging over random perturbations. The variance of ΔT is found to be

$$\sigma_T^2 = \langle (\Delta T)^2 \rangle = 2(\Delta\beta_1 l_c)^2[\exp(-L/l_c) + L/l_c - 1] \tag{3.17}$$

where $\Delta\beta 1 \equiv \Delta\tau/L$, $\Delta\tau$ represents the differential group delay along the principal states of polarization, and the correlation length l_c is defined as the length over which two polarization components remain correlated; typical values of l_c are of the order of 10 m. For $L > 0.1$ km, we can use $l_c \ll L$ to find that

$$\sigma_T \approx \Delta\beta_1\sqrt{2l_c L} \equiv D_P\sqrt{L} \tag{3.18}$$

where Dp is the PMD parameter. For most fibers, values of Dp are in the range of 0.1−1 ps/$\sqrt{km}$. Because of its $\sqrt{L}$ dependence, PMD-induced pulse broadening is relatively small compared with the GVD effects. However, PMD becomes a limiting factor for high-speed communication systems designed to operate over long distances near the zero-dispersion wavelength of the fiber. For some applications it is desirable that fibers transmit light without changing their state of polarization. Such fibers are called *polarization-maintaining* or polarization preserving fibers. A large amount of birefringence is introduced intentionally in these fibers through design modifications so that relatively small birefringence fluctuations are masked by it and do not affect the state of polarization significantly. One scheme breaks the cylindrical symmetry by making the fiber core elliptical in shape. The degree of birefringence achieved by this technique is typically $\sim 10^{-6}$. An alternative scheme makes use of stress-induced birefringence and permits Bm $\sim 10^{-4}$. In a widely adopted design, two rods of borosilicate glass are inserted on the opposite sides of the fiber core at the preform stage. The resulting birefringence depends on the location and the thickness of the stress-inducing elements. Figure 3.7 shows how Bm varies d for four shapes of stress-inducing elements located at a distance of five times the core radius. Values of Bm $\approx 2 \times 10^{-4}$ can be realized for d in the range of 50–60 μm. Such fibers are often named after the shape of the stress-inducing element, resulting in whimsical names such as “panda” and “bow-tie” fibers. The use of

polarization-maintaining fibers requires identification of the slow and fast axes before an optical signal can be launched into the fiber. Structural changes are often made to the fiber for this purpose. In one scheme, cladding is flattened in such a way that the flat surface is parallel to the slow axis of the fiber. Such a fiber is called the "D fiber" after the shape of the cladding and makes axes identification relatively easy. When the polarization direction of the linearly polarized light coincides with the slow or the fast axis, the state of polarization remains unchanged during propagation. In contrast, if the polarization direction makes an angle with these axes, polarization changes continuously along the fiber in a periodic manner with a period equal to the beat length [see Eq. (3.15)]. Figure 3.8 shows schematically the evolution of polarization over one beat length of a birefringent fiber. The state of polarization changes over one-half of the beat length from linear to elliptic, elliptic

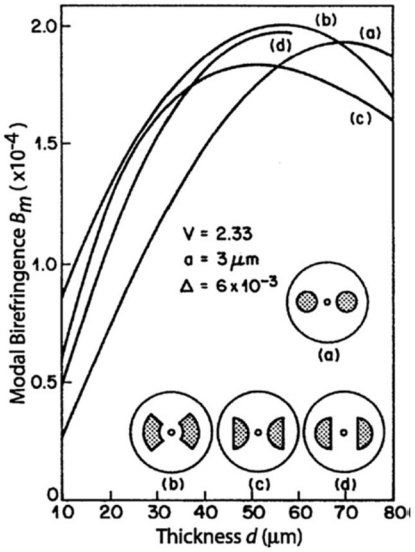

Figure 3.7 Variation of birefringence parameter *B*m with thickness *d* of the stress-inducing element for four different polarization-maintaining fibers. Different shapes of the stress applying elements (shaded region) are shown in the inset.

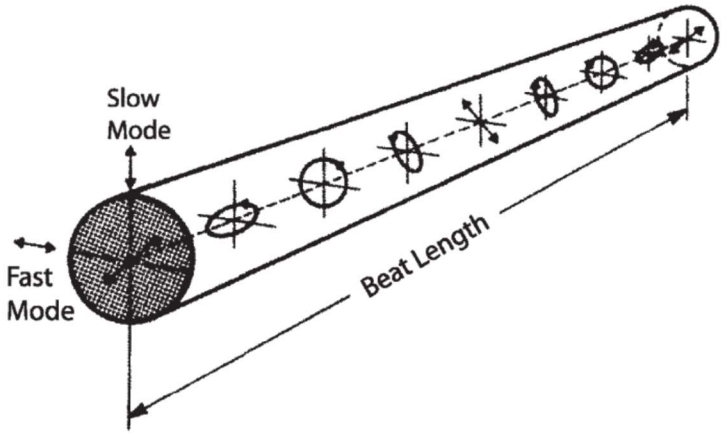

Figure 3.8 Evolution of the state of polarization along a polarization-maintaining fiber when the input signal is linearly polarized at 45° from the slow axis.

to circular, circular to elliptic, and then back to linear but is rotated by 90° from the incident linear polarization. The process is repeated over the remaining half of the beat length such that the initial state is recovered at $z = L_B$ and its multiples. The beat length is typically ∼1 m but can be as small as 1 cm for a strongly birefringent fiber with $B\text{m} \sim 10^{-4}$.

Chapter IV
Optical Fiber Modes

4.1.Introduction

An optical fiber is nominally a cylindrical dielectric waveguide that confines and guides light waves along its axis. Except for certain specialty fibers, basically all fibers used for telecommunication purposes have the same physical structure. The variations in the material and the size of this structure dictate how a light signal is transmitted along different types of fiber and also influence how the fiber responds to environmental perturbations, such as stress, bending, and temperature variations. This chapter describes various fiber structures, physical characteristics, operational properties, and applications.

4.2. Light Propagation in Fibers

Figure 4.1 shows the end-face cross section and a longitudinal cross section of a standard optical fiber, which consists of a cylindrical glass core surrounded by a glass cladding. The *core* has a refractive index n_1, and the *cladding* has a refractive index n_2. Surrounding these two layers is a polymer *buffer coating* that protects the fiber from mechanical and environmental effects. Traditionally the core radius is designated by the letter a. In almost all cases, for telecommunication fibers the core and cladding are made of silica glass (SiO_2).

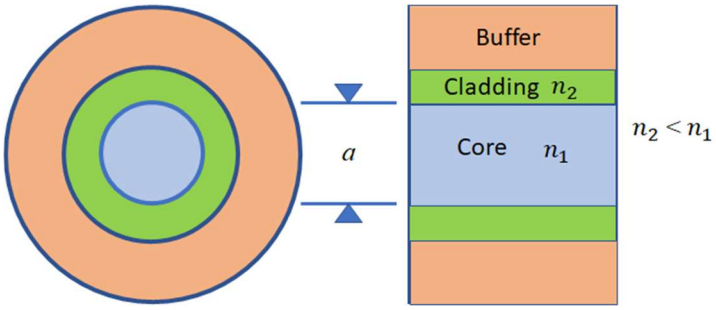

Figure 4.1. End-face cross section and a longitudinal cross section of a standard optical fiber.

The refractive index of pure silica varies with wavelength, ranging from 1.453 at 850 nm to 1.445 at 1550 nm. By adding certain impurities such as germanium or boron to the silica during the fiber manufacturing process, the index can be changed

slightly, usually as an increase in the core index. This is done so that the refractive index n_2 of the cladding is slightly smaller than the index of the core (that is, $n_2 < n_1$), which is the condition required for light traveling in the core to be totally internally reflected at the boundary with the cladding. The difference in the core and cladding indices also determines how light signals behave as they travel along a fiber. Typically, the index differences range from 0.2 to 3.0 percent depending on the desired behavior of the resulting fiber.

To get an understanding of how light travels along a fiber, let us first examine the case when the core diameter is much larger than the wavelength of the light. For such a case we can consider a simple geometric optics approach using the concept of light rays. Figure 4.2 shows a light ray entering the fiber core from a medium of refractive index n, which is less than the index n_1 of the core. The ray meets the core end face at an angle θ_0 with respect to the fiber axis and is refracted into the core. Inside the core the ray strikes the core-cladding interface at a normal angle ϕ. If the light ray strikes this interface at such an angle that it is totally internally reflected, then the ray follows a zigzag path along the fiber core.

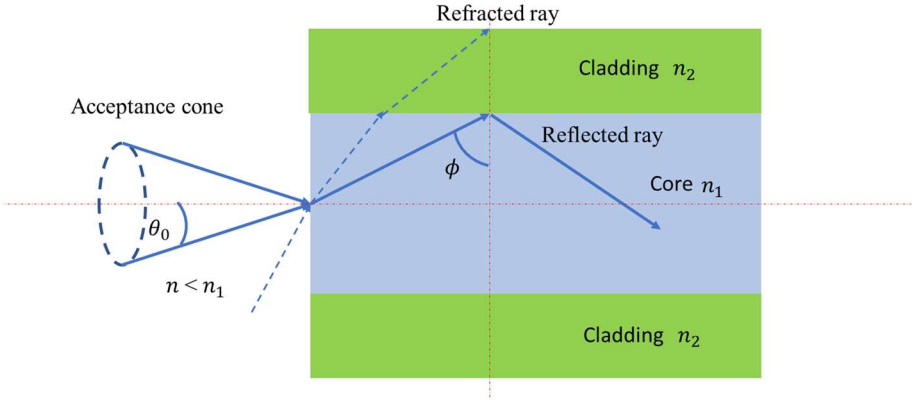

Figure 4.2. Ray optics representation of the propagation mechanism in an ideal step-index optical waveguide.

Now suppose that the angle θ_0 is the largest entrance angle for which total internal reflection can occur at the core-cladding interface. Then rays outside of the acceptance cone shown in Fig. 4.2, such as the ray given by the dashed line, will refract out of the core and be lost in the cladding. This condition defines a *critical angle* ϕ_c, which is the smallest angle ϕ that supports total internal reflection at the core-cladding interface.

4.2.1. Critical Angle

Referring to Fig. 4.2, from Snell's law the minimum angle $\phi = \phi_{min}$ that supports total internal reflection is given by

$$\phi_c = \phi_{min} = arcsin(n_2/n_1) \tag{4.1}$$

Rays striking the core-cladding interface at angles less than ϕ_{min} will refract out of the core and be lost in the cladding. Now suppose the medium outside of the fiber is air for which *n* = 1.00. By applying Snell's law to the air-fiber interface boundary, the condition for the critical angle can be related to the maximum entrance angle $\theta_{0,max}$ through the relationship

$$\sin\theta_{0,max} = n_1 \sin\theta_c = (n_1^2 - n_2^2)^{1/2} \tag{4.2}$$

Where $\theta_c = {}^{\pi}/_{2} - \phi_c$. Thus, those rays having entrance angles θ_0 less than $\theta_{0,max}$ will be totally internally reflected at the core-cladding interface.

Example

1. Suppose the core index $n_1 = 1.480$ and the cladding index n_2 =1.465. Then the critical angle is ϕ_c =arcsin (1.465/1.480) =82°, so that $\theta_c = {}^{\pi}/_{2} - \phi_c$ =8°.
2. With this critical angle, the maximum entrance angle is

$$\theta_{0,max} = arcsin(n_1 sin\theta_c) = arcsin(1.480\ sin8^o) = 11.9°$$

4.2.2. Optical Fiber Modes

Although it is not directly obvious from the ray picture shown in Fig. 4.2, only a finite set of rays at certain discrete angles greater than or equal to the critical angle ϕ_c is capable of propagating along a fiber. These angles are related to a set of electromagnetic wave patterns or field distributions called *modes* that can propagate along a fiber. When the fiber core diameter is on the order of 8 to 10 μm, which is only a few times the value of the wavelength, then only the one single *fundamental ray* that travels straight along the axis is allowed to propagate in a fiber. Such a fiber is referred to as a *single-mode fiber*. The operational characteristics of single-mode fibers cannot be explained by a ray picture, but instead need to be analyzed in terms of the *fundamental mode* by using the electromagnetic wave theory. Fibers with larger core diameters (e.g., greater than or equal to 50 μm) support many propagating rays or modes and are known as *multimode fibers*. A number of performance

characteristics of multimode fibers can be explained by ray theory whereas other attributes (such as the optical coupling concept) need to be described by wave theory. Figure 4.3 shows the field patterns of the three lowest-order *transverse electric* (TE) modes as seen in a cross-sectional view of an optical fiber. They are the TE_0, TE_1, and TE_2 modes and illustrate three of many possible power distribution patterns in the fiber core. The subscript refers to the *order* of the mode, which is equal to the number of zero crossings within the guide. In single-mode fibers only the lowest-order or *fundamental mode* (TE_0) will be guided along the fiber core. Its $1/e^2$ width is called the *mode field diameter*.

As the plots in Fig. 4.3 show, the power distributions are not confined completely to the core, but instead extend partially into the cladding. The fields vary harmonically within the core guiding region of index n_1 and decay exponentially outside of this region (in the cladding). For low-order modes the fields are concentrated tightly near the axis of the fiber with little penetration into the cladding. On the other hand, for higher-order modes the fields are distributed more toward the edges of the core and penetrate farther into the cladding region.

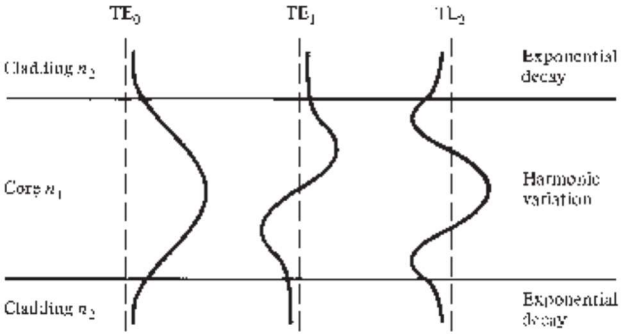

Figure 4.3. Electric field patterns of the three lowest-order guided modes as seen in a cross-sectional view of an optical fiber.

4.3. Variations of Fiber Types

Variations in the material composition of the core and the cladding give rise to the two basic fiber types shown in Fig. 4.4*a*. In the first case, the refractive index of the core is uniform throughout and undergoes an abrupt change (or step) at the cladding boundary. This is called a *step-index fiber*. In the second case, the core refractive index varies as a function of the radial distance from the center of the fiber. This defines a *graded-index fiber*. Figure 4.4*b* shows two of many different possible configurations.

Table 4.1 lists typical core, cladding, and buffer coating sizes of optical fibers for use in telecommunications, in a metropolitan-area network (MAN), or in a local-area network (LAN). The outer diameter of the buffer coating can be either 250 or 500 μm. Single-mode fibers are used for long-distance communication and for transmissions at very high data rates. The larger-core multimode fibers typically are used for local-area network applications in a campus environment, particularly for gigabit or 10-Gbit rate Ethernet links, which are known popularly as GigE and 10GigE, respectively. Here the word *campus* refers to any group of buildings that are within reasonable walking distance of one another.

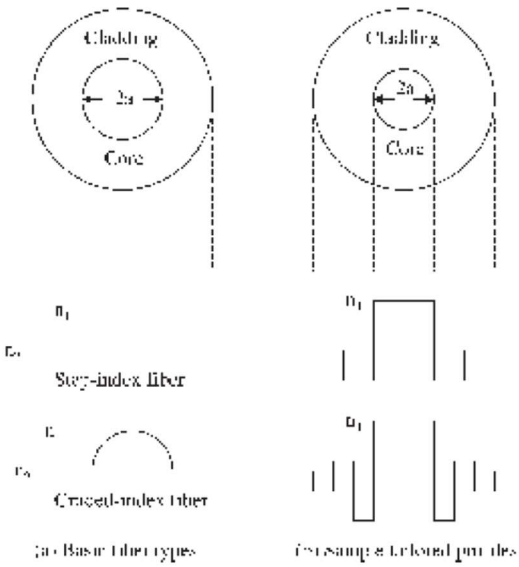

Figure 4.4. Variations in the material composition of the core and cladding yield different fiber types. (*a*) Simple profiles define step- and graded-index fibers; (*b*) complex cladding-index profiles tailor the signal dispersion characteristics of a fiber.

TABLE 4.1. Typical Core, Cladding, and Buffer Coating Sizes of Optical Fibers

Fiber type	Core diameter, μm	Cladding outer diameter, μm	Buffer outer diameter, μm	Application
Single-mode	7–10	125	250 or 500	Telecommunications
Multimode	50.0	125	250 or 500	LAN or MAN
Multimode	62.5	125	250 or 500	LAN
Multimode	85	125	250 or 500	Older LAN fiber
Multimode	100	140	250 or 500	Older fiber type

The critical angle also defines a parameter called the *numerical aperture* (NA), which is used to describe the light acceptance or gathering capability of fibers that have a core size much larger than a wavelength. This parameter defines the size of the acceptance cone shown in Fig. 4.2. The numerical aperture is a dimensionless quantity which is less than unity, with values ranging from 0.14 to 0.50.

4.3.1. Numerical Aperture

The critical angle condition on the entrance angle defines the *numerical aperture* (NA) of a step-index fiber. This is given by

$$NA = n \sin \theta_{0,max} = n_1 \sin \theta_c = (n_1^2 - n_2^2)^{1/2} \approx n_1 \sqrt{2 \triangle} \qquad (4.3)$$

where the parameter $\triangle$ is called the *core-cladding index difference* or simply the *index difference*. It is defined through the equation $n_2 = n_1(1 - \triangle)$. Typical values of $\triangle$ range from 1 to 3 percent for multimode fibers and from 0.2 to 1.0 percent for single-mode fibers. Thus, since $\triangle$ is much less than 1, the approximation on the right-hand side of the above equation is valid. Since the numerical aperture is related to the maximum acceptance angle, it is used commonly to describe the light acceptance or gathering capability of a multimode fiber and to calculate the source-to-fiber optical power coupling efficiencies.

Example A multimode step-index fiber has a core index n_1=1.480 and an index difference $\triangle = 0.01$. The numerical aperture for this fiber is $NA = 1.480\sqrt{0.02}$ =0.21.

4.4. Single-Mode Fibers

An important parameter for single-mode fibers is the *cutoff wavelength*. This is designated by λ_{cutoff} and specifies the smallest wavelength for which all fiber modes except the fundamental mode are cut off; that is, the fiber transmits light in a single mode only for those wavelengths that are greater than λ_{cutoff}. The fiber can support more than one mode if the wavelength of the light is less than the cutoff. Thus, if a fiber is single-mode at 1310 nm, it is also single-mode at 1550 nm, but not necessarily at 850 nm.

When a fiber is fabricated for single-mode use, the cutoff wavelength usually is chosen to be much less than the desired operating wavelength. For example, a fiber for single-mode use at 1310 nm may have a cutoff wavelength of 1275 nm.

4.4.1. Cutoff Wavelength

For a fiber to start supporting only a single mode at a wavelength λ_{cutoff}, the following condition (derived from solutions to Maxwell's equations for a circular waveguide) needs to be satisfied:

$$\lambda_{cutoff} = \frac{2\pi a}{2.405}(n_1^2 - n_2^2)^{1/2} \quad (4.4)$$

where a is the radius of the fiber core, n_1 is the core index, and n_2 is the cladding index.

Example Suppose we have a fiber with a = 4.2 μm, $n_1 = 1.480$, and $n_2 = n_1(1 - 0.0034) = 1.475$. Its cutoff wavelength then is

$$\lambda_{cutoff} = \frac{2\pi(4.2\mu m)}{2.405}(1.480^2 - 1.475^2)^{1/2} = 1334nm$$

4.5. Optical Fiber Attenuation

Light traveling in a fiber loses power over distance, mainly because of absorption and scattering mechanisms in the fiber. The fiber loss is referred to as *signal attenuation* or simply *attenuation*. Attenuation is an important property of an optical fiber because, together with signal distortion mechanisms, it determines the maximum transmission distance possible between a transmitter and a receiver (or an amplifier) before the signal power needs to be boosted to an appropriate level above the signal noise for high-fidelity reception. The degree of the attenuation depends on the wavelength of the light and on the fiber material. Figure 4.5 shows a typical attenuation versus wavelength curve for a silica fiber. The loss of power is measured in decibels, and the loss within a cable is described in terms of decibels per kilometer (dB/km).

Example

Suppose a fiber has an attenuation of 0.4 dB/km at a wavelength of 1310 nm. Then after it travels 50 km, the optical power loss in the fiber is 20 dB (a factor of 100). Figure 4.5 also shows that early optical fibers had a large attenuation spike between 900 and 1200 nm due to the fourth-order absorption peak from water molecules. Another spike from the third-order water absorption occurs between 1350 and 1480 nm for commonly fabricated fibers. Because of such absorption peaks, three transmission windows were defined initially. The *first window* ranges from 800 to 900 nm, the *second window* is centered at 1310 nm, and the *third window* ranges from 1480 to 1600 nm. Since the attenuation of low-waterpeak fibers makes the

designation of these windows obsolete, the concept of operational spectral bands arose for the 1260- to 1675-nm region. Figure 4.6 shows the attenuation as a function of wavelength for a low-water-peak fiber in the region covered by the six operational bands.

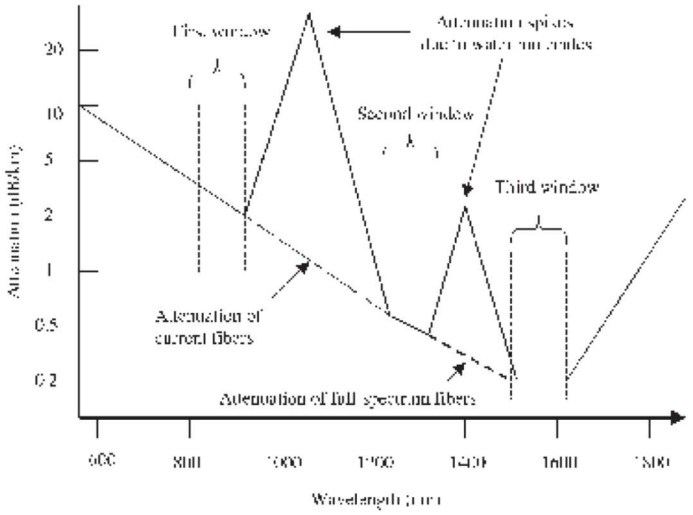

Figure 4.5. A typical attenuation versus wavelength curve for a silica fiber. Early fibers had a high loss spike around 1100 nm. Full-spectrum (low-water-content) fibers allow transmission in all spectral bands.

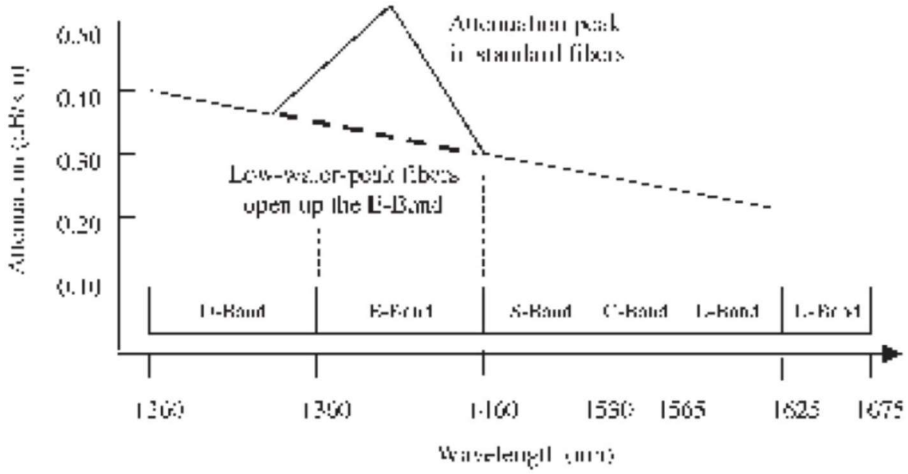

Figure 4.6. Attenuation versus wavelength for a low-water-peak fiber in the six operational spectral bands.

TABLE 4.2. Typical Losses in Standard 9-μm Fiber for Three Fiber Turns on a Specific Mandrel

Mandrel radius	Loss at 1310 nm	Loss at 1550 nm
1.15 cm	2.6 dB	23.6 dB
1.80 cm	0.1 dB	2.6 dB

In addition to the intrinsic absorption and scattering loss mechanisms in a fiber, light power can be lost as a result of fiber bending. Fibers can be subject to two types of bends: (1) *macroscopic bends* that have radii which are large compared with the fiber diameter, for example, those that occur when a fiber cable turns a corner, and (2) random *microscopic bends* of the fiber axis that can arise when fibers are incorporated into cables. Since the microscopic bending loss is determined in the manufacturing process, the user has little control over the degree of loss resulting from them. In general cable fabrication processes keep these values to a very low value, which is included in published cable loss specifications. For slight bends, the excess optical power loss due to macroscopic bending is extremely small and is essentially unobservable. As the radius of curvature decreases, the loss increases exponentially until at a certain critical bend radius the curvature loss becomes observable. If the bend radius is made a bit smaller once this threshold has been reached, the losses suddenly become extremely large. Bending losses depend on wavelength and are measured by winding several loops of fiber on a rod of a specific diameter. Table 4.2 gives typical bending loss values when three loops of a standard 9-μm core-diameter single-mode fiber are wound on rods with radii of 1.15 and 1.80 cm. Note the large difference in losses between operation at 1310 and 1550 nm. As a rule of thumb, it is best not to make the bend radius of such a fiber be less than 2.5 cm. Since often fibers need to be bent into very tight loops within component packages, special fibers that are immune to bending losses have been developed for such applications.

4.6. Fiber Information Capacity

The information-carrying capacity of the fiber is limited by various distortion mechanisms in the fiber, such as signal dispersion factors and nonlinear effects. The three main dispersion categories are modal, chromatic, and polarization mode dispersions. These distortion mechanisms cause optical signal pulses to broaden as

they travel along a fiber. As Fig. 4.7 shows, if optical pulses travel sufficiently far in a fiber, they will eventually overlap with neighboring pulses, thereby creating errors in the output since they become indistinguishable to the receiver. Nonlinear effects occur when there are high power densities (optical power per cross-sectional area) in a fiber. Their impact on signal fidelity includes shifting of power between wavelength channels, appearances of spurious signals at other wavelengths, and decreases in signal strength. *Modal dispersion* arises from the different path lengths associated with various modes (as represented by light rays at different angles). It appears only in multimode fibers, since in a single-mode fiber there is only one mode. By looking at Fig. 4.8 it can be deduced that rays bouncing off the core-cladding interface follow a longer path compared to the fundamental ray that travels straight down the fiber axis. For example, since ray 2 makes a steeper angle than ray 1, ray 2 has a longer path length from the beginning to the end of a fiber. If all the rays are launched into a fiber at the same time in a given light pulse, then they will arrive at the fiber end at slightly different times. This causes the pulse to spread out and is the basis of modal dispersion.

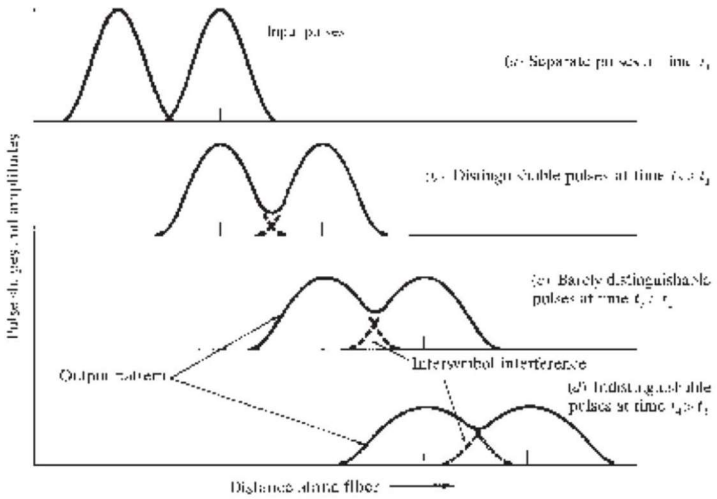

Figure 4.7. Broadening and attenuation of two adjacent pulses as they travel along a fiber.

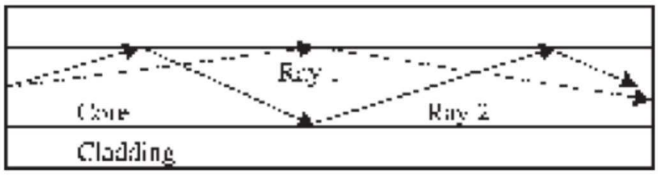

Figure 4.8. Rays that have steeper angles have longer path lengths.

ray 2 has a longer path length from the beginning to the end of a fiber. If all the rays are launched into a fiber at the same time in a given light pulse, then they will arrive at the fiber end at slightly different times. This causes the pulse to spread out and is the basis of modal dispersion. In a graded-index fiber, the index of refraction is lower near the core-cladding interface than at the center of the core. Therefore, in such a fiber the rays that strike this interface at a steeper angle will travel slightly faster as they approach the cladding than those rays arriving at a smaller angle. For example, this means that the light power in ray 2 shown in Fig. 4.8 will travel faster than that in ray 1. Thereby the various rays tend to keep up with one another to some degree. Consequently, the graded-index fiber exhibits less pulse spreading than a step-index fiber where all rays travel at the same speed. The index of refraction of silica varies with wavelength; for example, it ranges from 1.453 at 850 nm to 1.445 at 1550 nm. In addition, a light pulse from an optical source contains a certain slice of wavelength spectrum. For example, a laser diode source may emit pulses that have a 1-nm spectral width. Consequently, different wavelengths within an optical pulse travel at slightly different speeds through the fiber (s=c/n). Therefore, each wavelength will arrive at the fiber end at a slightly different time, which leads to pulse spreading. This factor is called *chromatic dispersion*, which often is referred to simply as *dispersion*. It is a fixed quantity at a specific wavelength and is measured in units of picoseconds per kilometer of fiber per nanometer of optical source spectral width, abbreviated as $ps/(km.nm)$. For example, a single-mode fiber might have a chromatic dispersion value of $D_{CD} = 2ps/(km.nm)$ at 1550 nm. Figure 4.9 shows the chromatic dispersion as a function of wavelength for several different fiber types, which are described in Sec. 4.8. *Polarization mode dispersion* (PMD) results from the fact that light-signal energy at a given wavelength in a single-mode fiber actually occupies two orthogonal polarization states or modes. Figure 4.10 shows this condition. At the start of the fiber the two polarization states are aligned. However, fiber material is not perfectly uniform throughout its length. In particular, the refractive index is not perfectly uniform across any given cross-sectional area. This condition is known as the *birefringence* of the material. Consequently, each polarization mode will encounter a slightly different refractive index, so that each will travel at a slightly different velocity and the polarization orientation will rotate with distance. The resulting difference in propagation times between the two orthogonal polarization modes will result in pulse spreading. This is the basis of polarization mode dispersion. PMD is not a fixed quantity but fluctuates

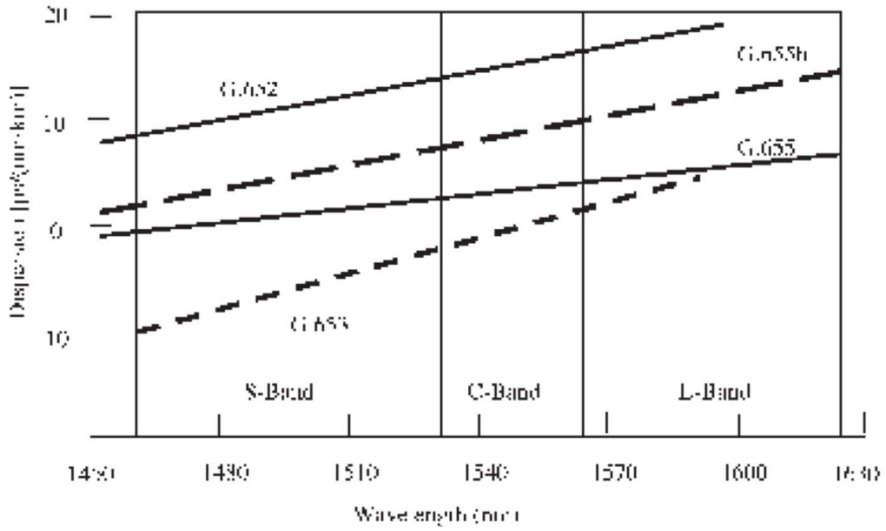

Figure 4.9. Chromatic dispersion as a function of wavelength in various spectral bands for several different fiber types.

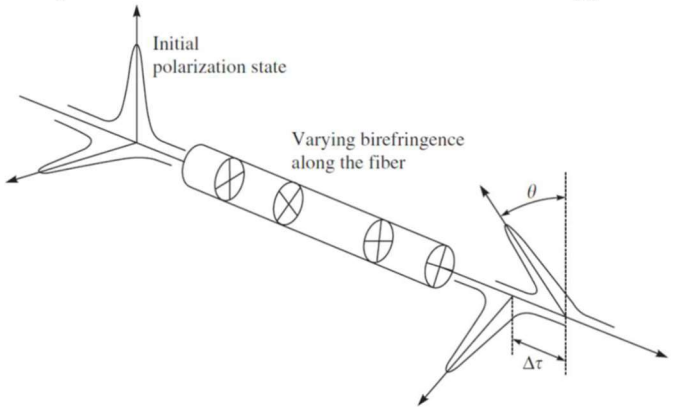

Figure 4.10. Variation in the polarization states of an optical pulse as it passes through a fiber that has varying birefringence along its length.

with time due to factors such as temperature variations and stress changes on the fiber. It varies as the square root of distance and thus is specified as a mean value in units of $ps/\sqrt{km}$. A typical value is $D_{PMD} = 0.05\, ps/\sqrt{km}$.

4.6.1. Dispersion Calculation

If t_{mod}, t_{CD}, and t_{PMD} are the modal, chromatic, and polarization mode dispersion times, respectively, then the total dispersion t_T can be calculated by the relationship

$$t_T = \sqrt{(t_{mod})^2 + (t_{CD})^2 + (t_{PMD})^2} \tag{4.5}$$

Note that $t_{mod} = 0$ for single-mode fibers. As a rule of thumb, the information carrying capacity over a certain length of fiber then is determined by specifying that the pulse spreading not be more than 10 percent of the pulse width at a designated data rate.

Example Consider a single-mode fiber for which $D_{CD} = 2\,ps/(km.nm)$ and $D_{PMD} = 0.1\,ps/\sqrt{km}$. If a transmission link has a length L = 500 km and uses a laser source with a spectral emission width of $\triangle\,\lambda = 0.01\,nm$, then we have $t_{mod} = 0$, $t_{CD} = D_{CD} \times L \times \triangle\,\lambda = 10pst$, and $t_{PMD} = D_{PMD} \times \sqrt{L} = 2.24\,ps$. Thus

$$t_T = \sqrt{(10ps)^2 + (2.24ps)^2} = 10.2\,ps$$

If t_T can be no more than 10 percent of a pulse width, then the maximum data rate R_{max} that can be sent over this 500-km link is $R_{max} = 0.1/t_T = 9.8Gbps$ (gigabits per second).

4.7. Optical Fiber Standards

The International Telecommunications Union (ITU-T) and the Telecommunications Industry Association (TIA/EIA) are the main organizations that have published standards for both multimode and single-mode optical fibers used in telecommunications. The recommended bounds on fiber parameters (e.g., attenuation, cutoff wavelength, and chromatic dispersion) designated in these standards ensure the users of product capability and consistency. In addition, the standards allow fiber manufacturers to have a reasonable degree of flexibility to improve products and develop new ones. Multimode fibers are used widely in LAN environments, storage area networks, and central-office connections, where the distance between buildings is typically 2 km or less. The two principal multimode fiber types for these applications have either 50- or 62.5-μm core diameters, and both have 125-μm cladding diameters. To meet the demands for short-reach low-cost transmission of high-speed Ethernet signals, a 50-μm multimode fiber is available for 10-Gbps operation at 850 nm over distances up to 300 m. Table 4.3 shows the operating ranges of various multimode fibers for applications up to 10GigE. The standards document TIA/EIA-568 lists the specifications for 10GigE fiber. The ITU-T recommendation G.651 describes other multimode fiber specifications for LAN applications using 850-nm optical sources. The ITU-T has published a series of recommendations for single-mode fibers. The characteristics of these fibers are given in the following listing. They are summarized in Table 4.4.

TABLE 4.6. Generic Parameter Values of an Erbium-Doped Fiber for Use in the C-Band

Parameter	Specification
Peak absorption at 1530 nm	5 to 10 dB/m
Effective numerical aperture	0.14 to 0.31
Cutoff wavelength	900 ± 50 nm; or 1300 nm
Mode field diameter at 1550 nm	5.0 to 7.3
Cladding diameter	125 μm standard; 80 μm for tight coils
Coating material	UV-cured acrylic

TABLE 4.4. ITU-T Recommendations for Single-Mode Fibers

ITU-T recommendation no.	Description
G.651	Multimode fiber for use at 850 nm in a LAN
G.652	Standard single-mode fiber (1310-nm optimized)
G.652.C	Low-water-peak fiber for CWDM applications
G.653	Dispersion-shifted fiber (made obsolete by NZDSF)
G.654	Submarine applications (1500-nm cutoff wavelength)
G.655	Nonzero dispersion-shifted fiber (NZDSF)
G.655b	Advanced nonzero dispersion-shifted fiber (A-NZDSF)

ITU-T G.652. This recommendation deals with the single-mode fiber that was installed widely in telecommunication networks in the 1990s. It has a Ge-doped silica core which has a diameter between 5 and 8 μm. Since early applications used 1310-nm laser sources, this fiber was optimized to have a zero-dispersion value at 1310 nm. Thus, it is referred to as a *1310-nm optimized fiber*. With the trend toward operation in the lower-loss 1550-nm spectral region, the installation of this fiber has decreased dramatically. However, the huge base of G.652 fiber that is installed worldwide will still be in service for many years. If network operators want to use installed G.652 fiber at 1550 nm, complex dispersion compensation techniques are needed, as described in Chap. 15.

ITU-T G.652.C. Low-water-peak fiber for CWDM applications is created by reducing the water ion concentration in order to eliminate the attenuation spike in the 1360- to 1460-nm E-band. The fibers have core diameters ranging from 8.6 to 9.5 μm and an attenuation of less than 0.4 dB/km. The main use of this fiber is for low-cost short-reach CWDM (coarse WDM) applications in the E-band. In CWDM

the wavelength channels are sufficiently spaced that minimum wavelength stability control is needed for the optical sources, as described in Chap. 13.

ITU-T G.653. *Dispersion-shifted fiber* (DSF) was developed for use with 1550-nm lasers. In this fiber type the zero-dispersion point is shifted to 1550 nm where the fiber attenuation is about one-half that at 1310 nm. Although this fiber allows a high-speed data stream of a single-wavelength channel to maintain its fidelity over long distances, it presents dispersion related problems in DWDM applications where many wavelengths are packed into one or more of the operational bands. As a result, this fiber type became obsolete with the introduction of G.655 NZDSF.

ITU-T G.654. This specification deals with *cutoff-wavelength-shifted fiber* that is designed for long-distance high-power signal transmission. Since it has a high cutoff wavelength of 1500 nm, this fiber is restricted to operation at 1550 nm. It typically is used only in submarine applications.

ITU-T G.655. *Nonzero dispersion-shifted fiber* (NZDSF) was introduced in the mid-1990s for WDM applications. Its principal characteristic is that it has a nonzero dispersion value over the entire C-band, which is the spectral operating region for erbium-doped optical fiber amplifiers (see Chap. 11). This is in contrast to G.653 fibers in which the dispersion varies from negative values through zero to positive values in this spectral range.

ITU-T G.655b. *Advanced nonzero dispersion-shifted fiber* (A-NZDSF) was introduced in October 2000 to extend WDM applications into the S-band. Its principal characteristic is that it has a nonzero dispersion value over the entire S-band and the C-band. This is in contrast to G.655 fibers in which the dispersion varies from negative values through zero to positive values in the S-band.

4.8. Specialty Fibers

Whereas telecommunication fibers, such as those described above, are designed to transmit light over long distances with minimal change in the signal, *specialty fibers* are used to manipulate the light signal. Specialty fibers interact with light and are custom-designed for specific applications such as optical signal amplification, wavelength selection, wavelength conversion, and sensing of physical parameters. A number of both passive and active optical devices use specialty fibers to direct, modify, or strengthen an optical signal as it travels through the device. Among these optical devices are light transmitters, optical signal modulators, optical receivers, wavelength multiplexers, couplers, splitters, optical amplifiers, optical switches,

wavelength add/drop modules, and light attenuators. Table 4.5 gives a summary of some specialty fibers and their applications.

4.8.1. Erbium-doped fiber

Erbium-doped optical fibers have small amounts of erbium ions added to the silica material and are used as a basic building block for optical fiber amplifiers. A length of Er-doped fiber ranging from 10 to 30m is used as a gain medium for amplifying optical signals in the C-band (1530 to 1560 nm). There are many variations on the doping level, cutoff wavelength, mode field diameter, numerical aperture, and cladding diameter for these fibers.

TABLE 4.5. Summary of Some Specialty Fibers and Their Applications

Specialty fiber type	Application
Erbium-doped fiber	Gain medium for optical fiber amplifiers
Photosensitive fibers	Fabrication of fiber Bragg gratings
Bend-insensitive fibers	Tightly looped connections in device packages
High-loss attenuating fiber	Termination of open optical fiber ends
Polarization-preserving fibers	Pump lasers, polarization-sensitive devices, sensors
High-index fibers	Fused couplers, short-λ sources, DWDM devices
Holey (photonic crystal) fibers	Switches; dispersion compensation

TABLE 4.6. Generic Parameter Values of an Erbium-Doped Fiber for Use in the C-Band

Parameter	Specification
Peak absorption at 1530 nm	5 to 10 dB/m
Effective numerical aperture	0.14 to 0.31
Cutoff wavelength	900 ± 50 nm; or 1300 nm
Mode field diameter at 1550 nm	5.0 to 7.3
Cladding diameter	125 μm standard; 80 μm for tight coils
Coating material	UV-cured acrylic

Higher erbium concentrations allow the use of shorter fiber lengths, smaller claddings are useful for compact packages, and a higher numerical aperture allows for the fiber to be coiled tighter in small packages. Table 4.6 lists some generic parameter values of an erbium-doped fiber for use in the C-band.

4.8.2. Photosensitive fiber. A photosensitive fiber is designed so that its refractive index changes when it is exposed to ultraviolet light. This sensitivity may be provided by doping the fiber material with germanium and boron ions. The main application is to create a fiber Bragg grating, which is a periodic variation of the refractive index along the fiber axis. Applications of fiber Bragg gratings include light-coupling mechanisms for pump lasers used in optical amplifiers, wavelength add/drop modules, optical filters, and chromatic dispersion compensation modules.

Bend-insensitive fiber. A bend-insensitive fiber has a moderately higher numerical aperture (NA) than that in a standard single-mode telecommunication fiber. The numerical aperture can be varied to adjust the mode field diameter. Increasing the NA reduces the sensitivity of the fiber to bending loss by confining optical power more tightly within the core than in conventional single-mode fibers. Bend-insensitive fibers are available commercially in a range of core diameters to provide optimum performance at specific operating wavelengths, such as 820, 1310, or 1550 nm. These fibers are offered with either an 80-μm or a 125-μm cladding diameter as standard products. The 80-μm *reduced-cladding fiber* results in a much smaller volume compared with a 125-μm cladding diameter when a fiber length is coiled up within a device package. Whereas Table 4.2 shows there is a high bending loss for tightly wound conventional single-mode fibers, the induced attenuation at the specified operating wavelength due to 100 turns of bend-insensitive fiber on a 10-mm-radius mandrel is less than 0.5 dB.

Attenuating fiber. These fibers have a uniform attenuation in the 1250- to 1620-nm band. This makes an attenuating fiber useful for WDM applications to lower the power level at the input of receivers or at the output of an EDFA. The fibers are offered commercially with attenuation levels available from 0.4 dB/cm to

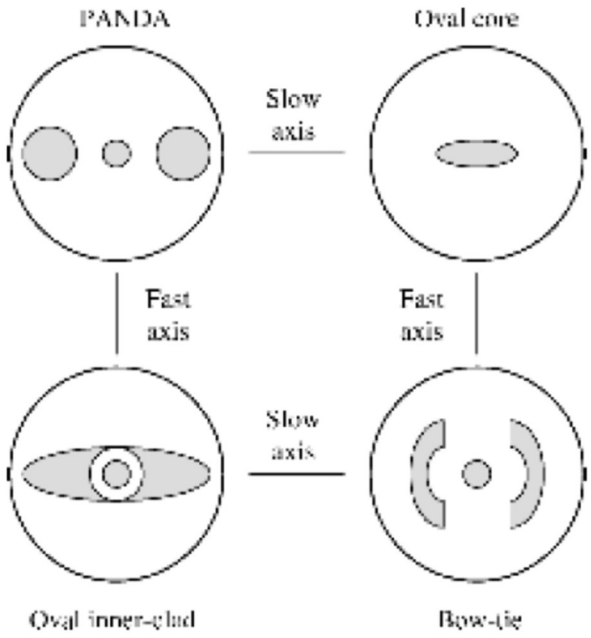

Figure 4.11. Cross-sectional geometry of four different polarization-maintaining fibers.

greater than 15 dB/cm. Fibers with an attenuation of 15 dB/cm (a loss factor of 32 within 1 cm) may be used to terminate the end of a fiber optic link so that there are no return reflections, or as a high-level plug-type attenuator.

Polarization-preserving fiber. In contrast to standard optical fibers in which the state of polarization fluctuates as a light signal propagates through the fiber, polarization-preserving fibers have a special core design that maintains the polarization. Applications of these fibers include light signal modulators fabricated from lithium niobate, optical amplifiers for polarization multiplexing, light-coupling fibers for pump lasers, and polarization-mode dispersion compensators. Figure 4.11 illustrates the cross-sectional geometry of four different polarization-maintaining fibers. The light circles represent the cladding, and the dark areas are the core configurations. The goal in each design is to introduce a deliberate birefringence into the core so that the two polarization modes become decoupled within a very short distance, which leads to preservation of the individual polarization states.

High-index fiber. These fiber types have a higher core refractive index, which results in a larger numerical aperture. Consequently, since a higher NA enables optical power to be coupled more efficiently into a core, a short (nominally 1-m) length of such a fiber may be attached directly to an optical source. Such a fiber

section is referred to as a *pigtail* or a *flylead*. The fibers can be designed specifically for short-wavelength or long-wavelength optical sources. In addition, they have applications in fused-fiber couplers and in wavelength division multiplexing.

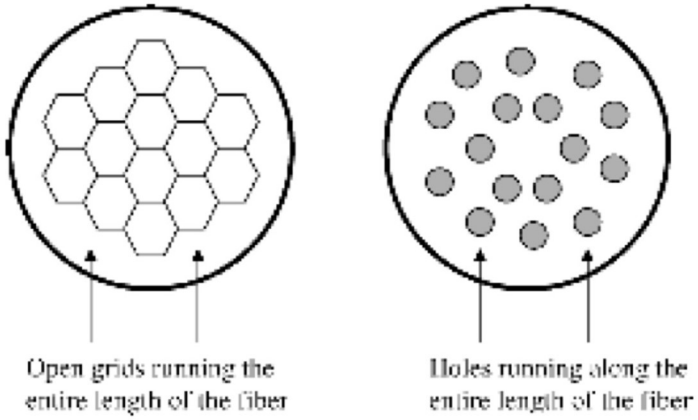

Figure 4.12. End-face patterns of two possible holey fiber structures.

Holey fiber. A holey or photonic crystal fiber typically consists of a silica material which contains numerous air-filled microscopic holes. Figure 4.12 shows the end-face patterns of two possible holey fiber structures. The tubular holes run along the entire length of the fiber parallel to the fiber axis. The size, position, and number of holes provide the fiber with specific waveguide properties. This technology is under development. Potential applications of holey fibers in telecommunications include dispersion compensation, wavelength conversion, optical switching, and high-power optical amplification.

Summary

An optical fiber is nominally a cylindrical dielectric waveguide that confines and guides light waves along its axis. Basically, all fibers used for telecommunication purposes have the same physical structure, which consists of a cylindrical glass core surrounded by a glass cladding. The difference in the core and cladding indices determines how light signals travel along a fiber. An important physical concept is that only a finite set of light rays that impinge on the core walls at specific angles may propagate along a fiber. These angles are related to a set of electromagnetic wave patterns called *modes*. For a *single-mode fiber,* the core diameter is around 8 to 10 μm (several wavelengths), and only the *fundamental ray* is allowed to propagate. *Multimode fibers* have larger core diameters (e.g., around 50 μm) and support many modes. The ray theory can explain a number of fiber performance

characteristics, but other attributes require the wave theory. The power distribution of modes is not confined completely to the core, but extends partially into the cladding. This concept is important when we examine concepts such as optical power coupling. Light traveling in a fiber loses power over distance, mainly because of absorption and scattering mechanisms in the fiber. This attenuation is an important property of an optical fiber because, together with signal distortion mechanisms, it determines the maximum transmission distance possible. The degree of the attenuation depends on the wavelength of the light and on the fiber material. The loss of power is measured in decibels, and the loss within a cable is described in terms of decibels per kilometer. The information-carrying capacity of the fiber is limited by various distortion mechanisms in the fiber, such as signal dispersion factors and nonlinear effects. The three main dispersion categories are modal, chromatic, and polarization mode dispersions. These distortion mechanisms cause optical signal pulses to broaden as they travel along a fiber. The ITU-T and the TIA/EIA have published standards for both multimode and single-mode optical fibers used in telecommunications. The recommended bounds on fiber parameters (e.g., attenuation, cutoff wavelength, and chromatic dispersion) designated in these standards ensure the users of product capability and consistency. Multimode fibers are used in LAN environments, storage area networks, and central-office connections, where the distance between buildings is typically 2 km or less. The two principal multimode fiber types have either 50- or 62.5-μm core diameters, and both have 125-μm cladding diameters. For short-reach, low-cost transmission of high-speed Ethernet signals, a 50-μm multimode fiber is available for 10-Gbps operation at 850 nm over distances up to 300 m. The ITU-T also has published a series of recommendations for single-mode fibers. Of these, two key ones for DWDM use are the ITU-T G.655 (nonzero dispersion-shifted fiber, or NZDSF) and the ITU-T G.655b (advanced nonzero dispersion-shifted fiber, or A-NZDSF). The G.655 fibers are designed for the C-band, and the G.655b fibers allow DWDM operation over the entire S-band and the C-band. In addition, the G.652.C recommendation describes fibers for CWDM applications. Whereas telecommunication fibers, such as those described above, are designed to transmit light over long distances with minimal change in the signal, *specialty fibers* are used to manipulate the light signal. Specialty fibers interact with light and are custom-designed for specific applications such as optical signal amplification, wavelength selection, wavelength conversion, and sensing of physical parameters.

Part II

LASER

Chapter V
Basic principle of LASER

5.1. Introduction

Although lasers were confined to the premises of prominent research centers such as the Bell laboratories, Hughes research laboratories and major academic institutes such as Columbia University in their early stages of development and evolution, this is no longer the case. Theodore Maiman demonstrated the first laser five decades ago in May 1960 at Hughes research laboratories. The acronym 'laser', Light Amplification by Stimulated Emission of Radiation, first used by Gould in his notebooks is a household name today. It was undoubtedly one of the greatest inventions of the second half of the 20^{th} century along with satellites, computers and integrated circuits; its unlimited application potential ensures that it continues to be so even today. Although lasers and laser technology are generally applied in commercial, industrial, bio-medical, scientific and military applications, the areas of its usage are multiplying as are the range of applications in each of these categories. This chapter, the first in Laser basics, is aimed at introducing the readers to operational fundamentals of lasers with the necessary dose of quantum mechanics. The topics discussed in this chapter include: the principles of laser operation; concepts of population inversion, absorption, spontaneous emission and stimulated emission; three-level and four-level lasers; basic laser resonator; longitudinal and transverse modes of operation; and pumping mechanisms.

5.2. Laser Operation

The basic principle of operation of a laser device is evident from the definition of the acronym 'laser', which describes the production of light by the stimulated emission of radiation. In the case of ordinary light, such as that from the sun or an electric bulb, different photons are emitted spontaneously due to various atoms or molecules releasing their excess energy unprompted. In the case of stimulated emission, an atom or a molecule holding excess energy is stimulated by a previously emitted photon to release that energy in the form of a photon. As we shall see in the following sections, population inversion is an essential condition for the stimulated emission process to take place. To understand how the process of population inversion subsequently leads to stimulated emission and laser action, a brief

summary of quantum mechanics and optically allowed transitions is useful as background information.

5.3. Rules of Quantum Mechanics

According to the basic rules of quantum mechanics all particles, big or small, have discrete energy levels or states. Various discrete energy levels correspond to different periodic motions of its constituent nuclei and electrons. While the lowest allowed energy level is also referred to as the ground state, all other relatively higher-energy levels are called excited states. As a simple illustration, consider a hydrogen atom. Its nucleus has a single proton and there is one electron orbiting the nucleus; this single electron can occupy only certain specific orbits. These orbits are assigned a quantum number N with the innermost orbit assigned the number $N = 1$ and the subsequent higher orbits assigned the numbers N=2, 3, 4 . . . outwards. The energy associated with the innermost orbit is the lowest and therefore $N = 1$ also corresponds to the ground state. Figure 1.1 illustrates the case of a hydrogen atom and the corresponding possible energy levels. The discrete energy levels that exist in any form of matter are not necessarily only those corresponding to the periodic motion of electrons. There are many types of energy levels other than the simple-to describe electronic levels. The nuclei of different atoms constituting the matter themselves have their own energy levels. Molecules have energy levels depending upon vibrations of different atoms within the molecule, and molecules also have energy levels corresponding to the rotation of the molecules. When we study different types of lasers, we shall see that all kinds of energy levels – electronic, vibrational and rotational – are instrumental in producing laser action in some of the very common types of lasers. Transitions between electronic energy levels of relevance to laser action correspond to the wavelength range from ultraviolet to near-infrared. Lasing action in neodymium lasers (1064 nm) and argon-ion lasers (488 nm) are some examples. Transitions between vibrational energy levels of atoms correspond to infrared wavelengths. The carbon dioxide laser (10600 nm) and hydrogen fluoride laser (2700 nm) are some examples. Transitions between rotational energy levels correspond to a wavelength range from 100 microns (mm) to 10 mm.

In a dense medium such as a solid, liquid or high-pressure gas, atoms and molecules are constantly colliding with each other thus causing atoms and molecules to jump from one energy level to another. What is of interest to a laser scientist however is

an optically allowed transition. An optically allowed transition between two energy levels is one that involves either absorption or emission of a photon which satisfies the resonance condition of $\Delta E = h\nu$, where ΔE is the difference in energy between the two involved energy levels, h is Planck's constant (= 6.6260755 x10^{-34} J s or 4.1356692x10^{-15} eV s) and ν is frequency of the photon emitted or absorbed.

5.4. Absorption, Spontaneous Emission and Stimulated Emission

Absorption and emission processes in an optically allowed transition are briefly mentioned in the previous section. An electron or an atom or a molecule makes a transition from a lower energy level to a higher energy level only if suitable conditions exist. These conditions include:

1. the particle that has to make the transition should be in the lower energy level; and
2. the incident photon should have energy ($= h\nu$) equal to the transition energy, which is the difference in energies between the two involved energy levels, that is

$$\Delta E = h\nu \tag{5.1}$$

If the above conditions are satisfied, the particle may make an absorption transition from the lower level to the higher level (Figure 5.2a). The probability of occurrence of such a transition is proportional to both the population of the lower level and also the related Einstein coefficient. There are two types of emission processes, namely: spontaneous emission and stimulated emission. The emission process, as outlined above, involves transition from a higher excited energy level to a lower energy level. Spontaneous emission is the phenomenon in which an atom or molecule undergoes a transition from an excited higher-energy level to a lower level without any outside intervention or stimulation, emitting a resonance photon in the process (Figure 5.2b). The rate of the spontaneous emission process is proportional to the related Einstein coefficient. In the case of stimulated emission (Figure 5.2c), there first exists a photon referred to as the stimulating photon which has energy equal to the resonance energy ($h\nu$). This photon perturbs another excited species (atom or molecule) and causes it to drop to the lower energy level, emitting a photon of the same frequency, phase and polarization as that of the stimulating photon in the process. The rate of the stimulated emission process is proportional to the population of the higher excited energy level and the related Einstein coefficient. Note that, in the case of spontaneous emission, the rate of the emission

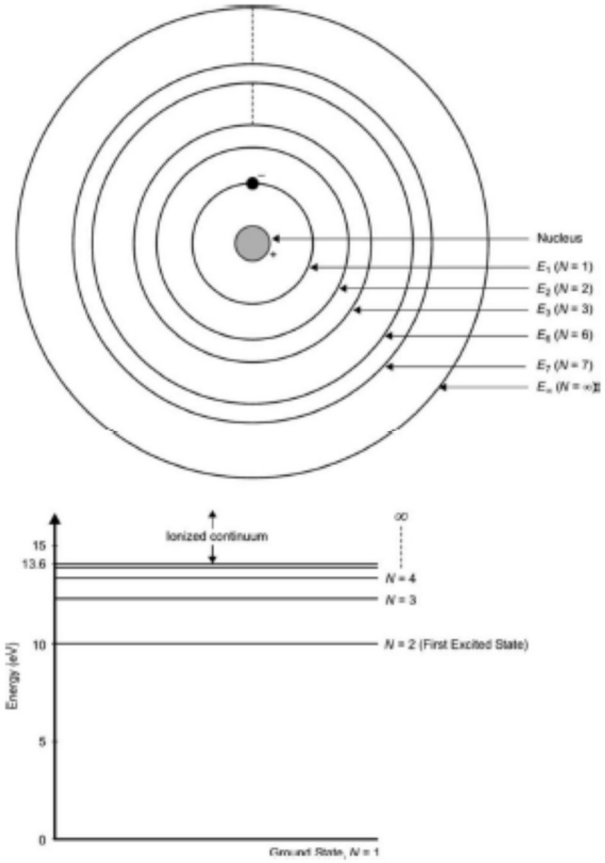

Figure 5.1 Energy levels associated with the hydrogen atom.

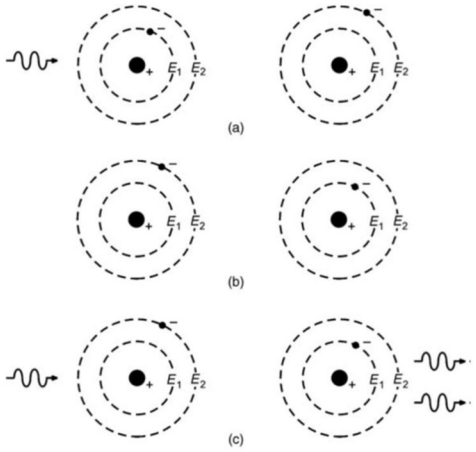

Figure 5.2 Absorption and emission processes: (a) absorption; (b) spontaneous emission; and (c) stimulated emission.

process does not depend upon the population of the energy state from where the transition has to take place, as is the case in absorption and stimulated emission processes. According to the rules of quantum mechanics, absorption and stimulated emission are analogous processes and can be treated similarly. We have seen that absorption, spontaneous emission and stimulated emission are all optically allowed transitions. Stimulated emission is the basis for photon multiplication and the fundamental mechanism underlying all laser action. In order to arrive at the necessary and favorable conditions for stimulated emission and set the criteria for laser action, it is therefore important to analyze the rates at which these processes are likely to occur. The credit for defining the relative rates of these processes goes to Einstein, who determined the well-known 'A' and 'B' constants known as Einstein's coefficients. The 'A' coefficient relates to the spontaneous emission probability and the 'B' coefficient relates to the probability of stimulated emission and absorption. Remember that absorption and stimulated emission processes are analogous phenomenon. The rates of absorption and stimulated emission processes also depend upon the populations of the lower and upper energy levels, respectively. For the purposes of illustration, consider a two-level system with a lower energy level 1 and an upper excited energy level 2 having populations of N_1 and N_2, respectively, as shown in Figure 5.3a. Einstein's coefficients for the three processes are B_{12} (absorption), A_{21} (spontaneous emission) and B_{21} (stimulated emission). The subscripts of the Einstein coefficients here represent the direction of transition. For instance, B_{12} is the Einstein coefficient for transition from level 1 to level 2. Also, since absorption and stimulated emission processes are analogous according to laws of quantum mechanics, $B_{12} = B_{21}$. According to Boltzmann statistical thermodynamics, under normal conditions of thermal equilibrium atoms and molecules tend to be at their lowest possible energy level, with the result that population decreases as the energy level increases. If E_1 and E_2 are the energy levels

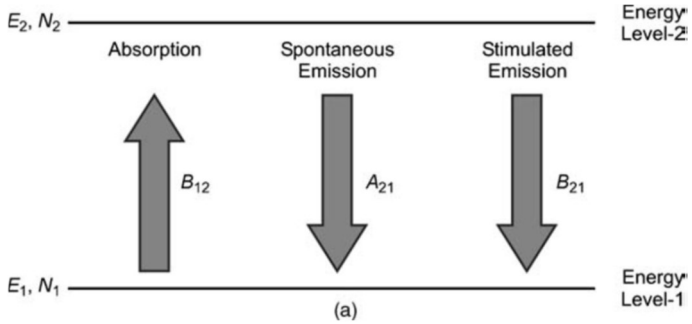

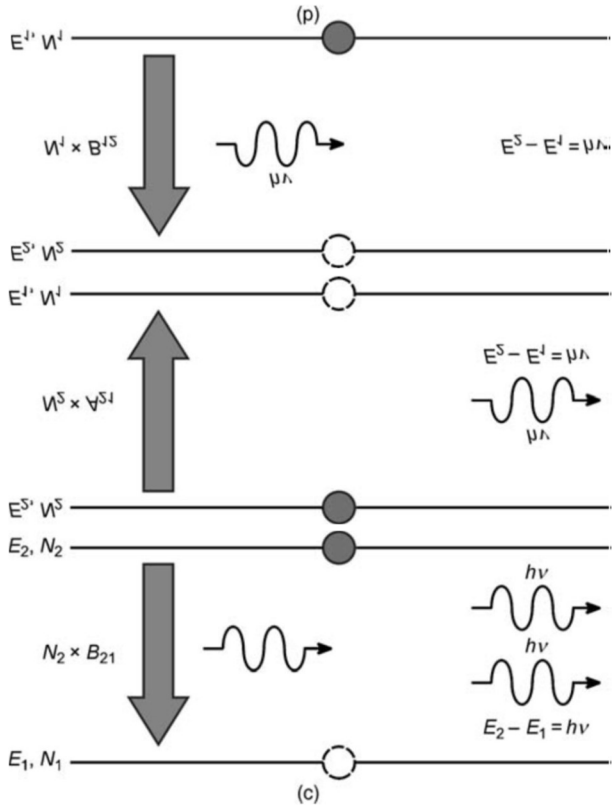

Figure 5.3 Absorption, spontaneous emission and stimulated emission.

associated with level 1 and level 2, respectively, then the populations of these two levels can be expressed by Equation 5.2:

$$\frac{N_2}{N_1} = \exp[-(E_2 - E_1)/kT] \quad (5.2)$$

Where

k = Boltzmann constant=$1.38 \times 10^{-23} JK^{-1}$ or $8.6 \times 10^{-23} eVK^{-1}$

T= absolute temperature in degrees Kelvin

Under normal conditions, N_1 is greater than N_2. When a resonance photon ($\Delta E = h\nu$) passes through the species of this two-level system, it may interact with a particle in level 1 and become absorbed, in the process raising it to level 2. The probability of occurrence of this is given by $B_{12} \times N_1$ (Figure 5.3b). Alternatively, it may interact with a particle already in level 2, leading to emission of a photon with the same frequency, phase and polarization. The probability of occurrence of this process, known as stimulated emission, is given by $B_{21} \times N_2$ (Figure 5.3d). Yet another possibility is that a particle in the excited level 2 may drop to level 1 without any outside intervention, emitting a photon in the process. The probability of this spontaneous emission is A_{21} (Figure 5.3c). The spontaneously emitted photons have

the same frequency but have random phase, propagation direction and polarization. If we analyze the competition between the three processes, it is clear that if $N_2 > N_1$ (which is not the case under the normal conditions of thermal equilibrium), there is the possibility of an overall photon amplification due to enhanced stimulated emission. This condition of $N_2 > N_1$ is known as population inversion since $N_1 > N_2$ under normal conditions. We shall explain in the following sections why population inversion is essential for a sustained stimulated emission and hence laser action.

Example 5.1

Refer to Figure 1.4. It shows the energy level diagram of a typical neodymium laser. If this laser is to be pumped by flash lamp with emission spectral bands of 475–525 nm, 575–625 nm, 750–800 nm and 820–850 nm, determine the range of emission wavelengths that would be absorbed by the active medium of this laser and also the wavelength of the laser emission.

Solution

1. Referring to the energy level diagram of Figure 1.4, two edges of the absorption band correspond to energy levels of $12500\ cm^{-1}$ and $13330\ cm^{-1}$. Corresponding wavelengths (of photons) that would have these energy levels are computed as:

Wavelength corresponding to $12500\ cm^{-1} = (1/12500)cm = (10^7/12500)nm = 800\ nm$

Wavelength corresponding to $13330\ cm^{-1} = (1/13330)cm = (10^7/13330)nm = 750.19\ nm \cong 750\ nm$

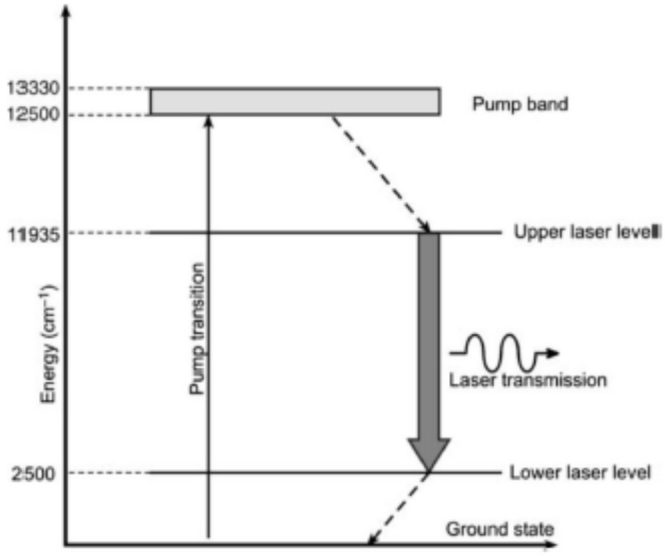

Fig 5.4: Energy level diagram.

2. The absorption band of the active medium is therefore 750–800 nm. This is the band of wavelengths that would be absorbed by the active medium.
3. Lasing action takes place between metastable energy level $11935\ cm^{-1}$ and the lower energy level $2500\ cm^{-1}$. The difference between two energy levels is $11935 - 2500\ cm^{-1} = 9435\ cm^{-1}$.
4. This energy corresponds to a wavelength of $(1/9435)cm = (10^7/9435)nm = 1059.88\ nm \cong 1060\ nm$.
5. The emitted laser wavelength is therefore = 1060 nm.

Example 5.2
Figure 5.5 shows the energy level diagram of a popular type of a gas laser. Determine the possible emission wavelengths.
Solution
1. The emission wavelength is such that the corresponding energy value equals the energy difference between the involved lasing levels.
2. **For emission 1**, the energy difference (from Figure 5.5) = 0.117 eV.
If λ_1 is the emission wavelength, then $hc/\lambda_1 = 0.117\ eV$ where
$h =$ Planck's constant $= 6.6260755 \times 10^{-3}$ J s or $4.1356692 \times 10^{-15}$eV s
$c = 3 \times 10^{10}\ cms^{-1}$
Substituting these values, $\lambda_1 = (4.1356692 \times 10^{-15} \times 3 \times 10^{10})/0.117\ cm = 106.04 \times 10^{-5}\ cm = 10604\ nm$.
3. **For emission 2**, the energy difference (from Figure 5.5) = 0.129 eV
If λ_1 is the emission wavelength, then $hc/\lambda_1 = 0.129\ eV$. Substituting these values, $\lambda_1 = (4.1356692 \times 10^{-15} \times 3 \times 10^{10})/0.129\ cm = 96.178 \times 10^{-5}\ cm = 9617.8\ nm$.
4. The energy level diagram shown in Figure 5.5 is that of carbon dioxide laser, which is also evident from the results obtained for the two emission wavelengths.

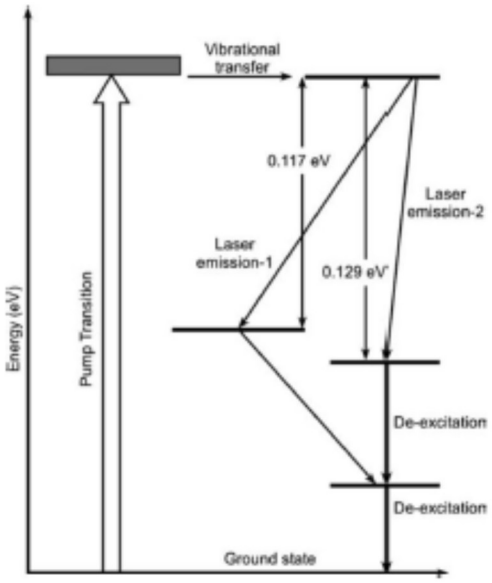

Fig 5.5: Energy level diagram.

Example 5.3

We know that absorption and emission between two involved energy levels takes place when the photon energy corresponding to the absorbed or emitted wavelength equals the energy difference between the two energy levels. If ΔE is energy difference in eV, prove that the absorbed or emitted wavelength (in nm) approximately equals ($1240/\Delta E$).

Solution

1. Emitted or absorbed wavelength $\lambda = hc/\Delta E$

2. In the above expression, if we substitute the value of h in eV s, c in $nm\ s^{-1}$ and ΔE in eV, we obtain λ in nm.

3. Now, $h = 4.1356692 \times 10^{-15}$eV s and $c = 3 \times 10^{8}\, ms^{-1} = c = 3 \times 10^{17}\, nms^{-1}$ _1¼3_1017 nms_1

Therefore, $\lambda\ (in\ nm) = 4.1356692 \times 10^{-15} \times 3 \times 10^{17}/\Delta E \cong 1240/\Delta E$.

Conclusion

Lasers were undoubtedly one of the greatest inventions of the second half of 20th century – along with satellites, computers and integrated circuits – and continue to be so today due to their unlimited application potential. The basic principle of operation of a laser device is based on stimulated emission of radiation. In the case of ordinary light, such as that from the sun or an electric bulb, different photons are

emitted spontaneously due to various atoms or molecules releasing their excess energy. In the case of stimulated emission, an atom or a molecule holding excess energy is stimulated by another previously emitted photon to release that energy in the form of a photon. A laser scientist is interested in an optically allowed transition between two energy levels, which involves either absorption or emission of a photon satisfying the resonance condition of $\Delta E = h\nu$ where ΔE is the difference in energy between the two involved energy levels, h is Planck's constant $= 6.6260755 \times 10^{-3}$ J s or 4.1356692×10^{-1} eV s) and n is the frequency of the photon emitted or absorbed. There are two types of emission processes: spontaneous emission and stimulated emission. The emission process involves transition from a higher excited energy level to a lower energy level. Spontaneous emission is the phenomenon in which an atom or molecule undergoes a transition from an excited higher energy level to a lower level without any outside intervention or stimulation, emitting a resonance photon in the process.

Chapter VI
Population Inversion

6.1. Introduction

We shall illustrate the concept of population inversion with the help of the same two-level system considered above. If we compute the desired transition energy for an optically allowed transition, let us say at a wavelength of 1064 nm corresponding to the output wavelength of a neodymium-doped yttrium aluminum garnet (Nd:YAG) laser, it turns out to be about 1 eV (transition energy $\Delta E = h\nu$). For a transition energy of 1 eV, we can now determine the population N_2 of level 2, which is the upper excited level here, for a known population N_1 of the lower level at room temperature of 300 K from Equation 5.2. The final relationship is $N_2 = 1.5 \times 10^{-17} N_1$. This implies that practically all atoms or molecules are in the lower level under thermodynamic equilibrium conditions. Let us not go that far and instead consider a situation where the population of the lower level is only ten times that of the excited upper level. We shall now examine what happens when there is a spontaneously emitted photon. Now there are two possibilities: either this photon stimulates another excited species in the upper level to cause emission of another photon of identical character, or it would hit an atom or molecule in the lower level and be absorbed. Since there are 10 atoms or molecules in the lower level for every excited species in the upper level, we can say that 10 out of every 11 spontaneously emitted photons hit the atoms or molecules in the lower level and become absorbed. Only 9% (1 out of every 11) of the photons can cause stimulated emission. The photons emitted by the stimulated process will also become absorbed successively due to the scarcity of excited species in the upper level. Another way of expressing this is that when the population of the lower level is much larger than the population of the excited upper level, the probability of each spontaneously emitted photon hitting an atom or molecule in the lower level and becoming absorbed is also much higher than the same stimulating another excited atom or molecule in the upper level. The same concept underlies the expressions for the probability of absorption, spontaneous emission and stimulated emission previously outlined in Section 1.4:

Probability of absorption $= B_{12} \times N_1$

Probability of spontaneous emission $= A_{12}$

Probability of stimulated emission $= B_{21} \times N_2$

If we want the stimulated emission to dominate over absorption and spontaneous emission, we must have a greater number of excited species in the upper level than the population of the lower level. Such a situation is known as population inversion since under normal circumstances the population of the lower level is much greater than the population of the upper level. Population inversion is therefore an essential condition for laser action. The next obvious question is that of the desired extent of population inversion. Spontaneous emission depletes the excited upper-level population (N_2 in the present case) at a rate proportional to A_{21} producing undesired photons with random phase, direction of propagation and polarization. Due to this loss and other losses associated with laser cavity (discussed in Section 1.7), each laser has a certain minimum value of $N_2 - N_1$ for the production of laser output. This condition of population inversion is known as the inversion threshold of the laser. Lasing threshold is an analogous term.

Next, we shall discuss how we can produce population inversion.

6.2. Producing Population Inversion

That population inversion is an essential condition for laser action is demonstrated above. Population inversion ensures that there are more emitters than absorbers with the result that stimulated emission dominates over spontaneous emission and absorption processes. There are two possible ways to produce population inversion. One is to populate the upper level by exciting extra atoms or molecules to the upper level. The other is to depopulate the lower laser level involved in the laser action. In fact, for a sustained laser action, it is important to both populate the upper level and depopulate the lower level. Two commonly used pumping or excitation mechanisms include optical pumping and electrical pumping. Both electrons and photons have been successfully used to create population inversion in different laser media. While optical pumping is ideally suited to solid-state lasers such as ruby, Nd:YAG and neodymium-doped glass (Nd:Glass) lasers, electrical discharge is the common mode of excitation in gas lasers such as helium-neon and carbon dioxide lasers. The excitation input, optical or electrical, usually raises the atoms or molecules to a level higher than the upper laser level from where it rapidly drops to the upper laser level. In some cases, the excitation input excites atoms other than the active species. The excited atoms then transfer their energy to the active species to cause population inversion. A helium-neon laser is a typical example of this kind where the excitation input gives its energy to helium atoms, which subsequently transfer the energy to neon atoms to raise them to the upper laser level. The other important concept

essential for laser action is the existence of a metastable state as the upper laser level. For stimulated emission, the excited state needs to have a relatively longer lifetime of the order of a few microseconds to a millisecond or so. The excited species need to stay in the excited upper laser level for a longer time in order to allow interaction between photons and excited species, which is necessary for efficient stimulated emission. If the upper laser level had a lifetime of a few nanoseconds, most of the excited species would drop to the lower level as spontaneous emission. The crux is that, for efficient laser action, the population build-up of the upper laser level should be faster than its decay. A longer upper laser level lifetime helps to achieve this situation.

6.3. Two, Three and Four Level Laser Systems

Another important feature that has a bearing on the laser action is the energy level structure of the laser medium. As we shall see in the following sections, energy level structure, particularly the energy levels involved in the population inversion process and the laser action, significantly affect the performance of the laser.

6.3.1. Two-Level Laser System

In a two-level laser system, there are only two levels involved in the total process. The atoms or molecules in the lower level, which is also the lower level of the laser transition, are excited to the upper level by the pumping or excitation mechanism. The upper level is also the upper laser level. Once the population inversion is achieved and its extent is above the inversion threshold, the laser action can take place. Figure 6.1 shows the arrangement of energy levels in a two-level system. A two-level system is, however, a theoretical concept only as far as lasers are concerned. No laser has ever been made to work as a two-level system.

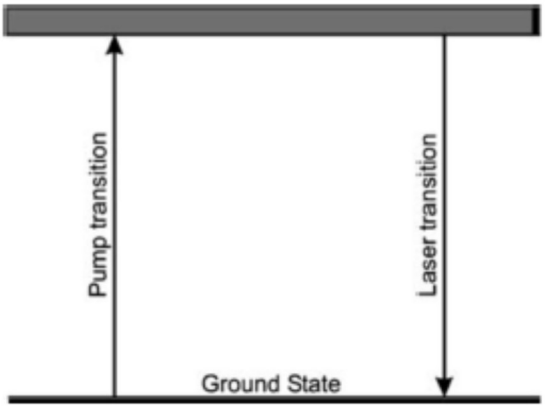

Figure 6.1 Two-level laser system.

6.3.2. Three-Level Laser System

In a three-level laser system, the lower level of laser transition is the ground state (the lowermost energy level). The atoms or molecules are excited to an upper level higher than the upper level of the laser transition (Figure 6.2). The upper level to which atoms or molecules are excited from the ground state has a relatively much shorter lifetime than that of the upper laser level, which is a metastable level. As a result, the excited species rapidly drop to the metastable level. A relatively much longer lifetime for the metastable level ensures a population inversion between the metastable level and the ground state provided that more than half of the atoms or molecules in the ground state have been excited to the uppermost short-lived energy level. The laser action occurs between the metastable level and the ground state. A ruby laser is a classic example of a three-level laser. Figure 6.3 shows the energy level structure for this laser. One of the major shortcomings of this laser and other three-level lasers is due to the lower laser level being the ground state. Under thermodynamic equilibrium conditions, almost all atoms or molecules are in the ground state and so it requires more than half of this number to be excited out of the ground state to achieve laser action. This implies that a much larger pumping input would be required to exceed population inversion threshold. This makes it very difficult to sustain population inversion on a continuous basis in three-level lasers. That is why a ruby laser cannot be operated in continuous-wave (CW) mode.

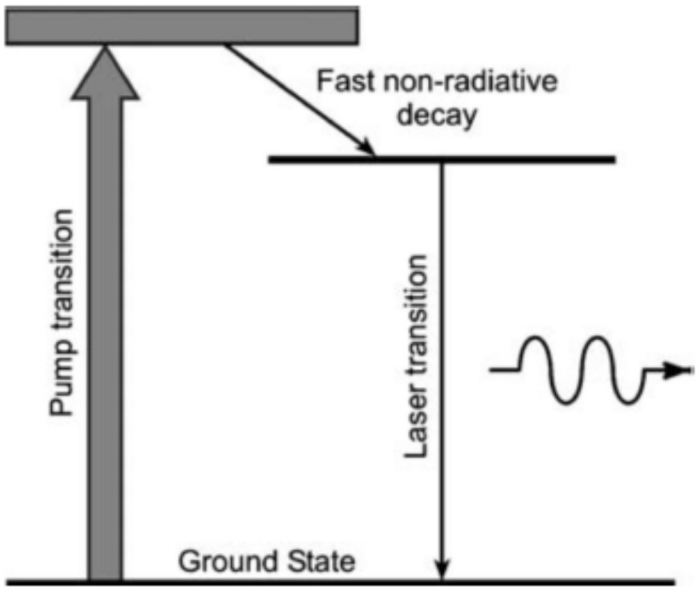

Fig 6.2 Three-level laser system.

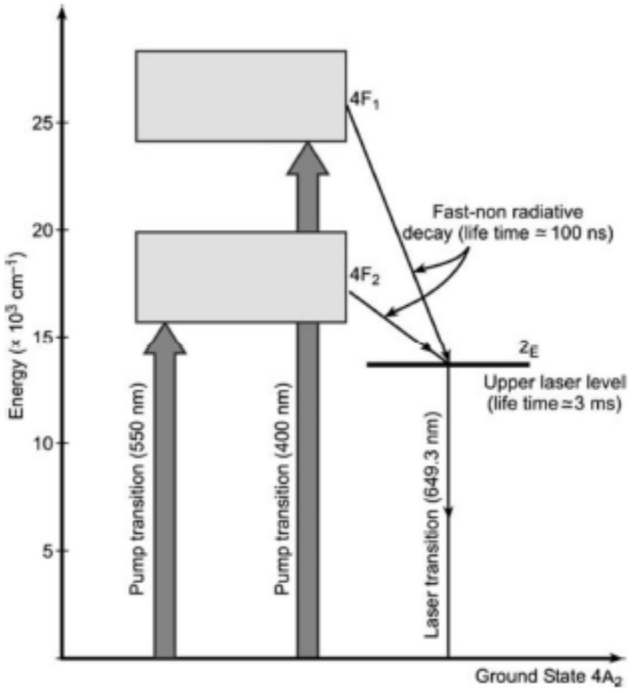

Fig 6.3 Energy level diagram of ruby laser.

An ideal situation would be if the lower laser level were not the ground state so that it had much fewer atoms or molecules in the thermodynamic equilibrium condition, solving the problem encountered in three-level laser systems. Such a desirable situation is possible in four-level laser systems in which the lower laser level is above the ground state, as shown in Figure 6.4.

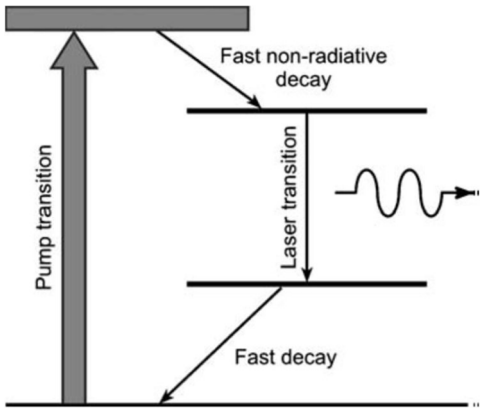

Figure 6.4 Four-level laser system.

6.3.3. Four-Level Laser System

In a four-level laser system, the atoms or molecules are excited out of the ground state to an upper highly excited short-lived energy level. Remember that the lower laser level here is not the ground state. In this case, the number of atoms or molecules required to be excited to the upper level would depend upon the population of the lower laser level, which is much smaller than the population of the ground state. Also if the upper level to which the atoms or molecules are initially excited and the lower laser level have a shorter lifetime and the upper laser level (metastable level) a longer lifetime, it would be much easier to achieve and sustain population inversion. This is achievable due to two major features of a four-level laser. One is rapid population of the upper laser level, which is a result of an extremely rapid dropping of the excited species from the upper excited level where they find themselves with excitation input to the upper laser level accompanied by the longer lifetime of the upper laser level. The second occurrence is the depopulation of the lower laser level due to its shorter lifetime. Once it is simpler to sustain population inversion, it becomes easier to operate the laser in the continuous-wave (CW) mode. This is one of the major reasons that a four level laser such as an Nd:YAG laser or a helium-neon laser can be operated in the continuous mode while a three-level laser such as a ruby laser can only be operated as a pulsed laser.

Nd:YAG, helium-neon and carbon dioxide lasers are some of the very popular lasers with a four-level energy structure. Figure 6.5 shows the energy level structure of a Nd:YAG laser. The pumping or excitation input raises the atoms or molecules to the uppermost energy level, which in fact is not a single level but instead a band of energy levels. This is a highly desirable feature, the reason for which is discussed more fully in Section 1.11 on pumping mechanisms. The excited species rapidly fall to the upper laser level (metastable level). This decay time is about 100 ns. The metastable level has a

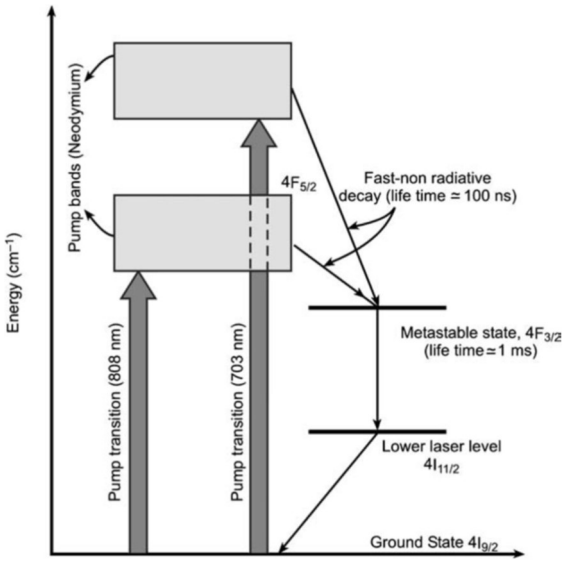

Fig 6.5 Energy level diagram of Nd:YAG laser.

metastable lifetime of about 1 ms and the lower laser level has a decay time of 30 ns. If we compare the four-level energy level structure of a Nd:YAG laser with that of a neodymium-doped yttrium lithium fluoride (Nd:YLF) laser, another solid-state laser with a four-level structure, we find that there is a striking difference in the lifetime of the metastable level. Nd:YLF has a higher metastable lifetime (typically a few milliseconds) as compared to 1 ms of Nd:YAG. This gives the former a higher storage capacity for the excited species in the metastable level. In other words, this means that a Nd:YLF rod could be pumped harder to extract more laser energy than a Nd:YAG rod of the same size.

6.4. Energy Level Structures of Practical Lasers

In the case of real lasers, the active media do not have the simple three- or four-level energy level structures as described above, but are far more complex. For instance, the short-lived uppermost energy level, to which the atoms or molecules are excited out of the ground state and from where they drop rapidly to the metastable level, is not a single energy level. It is in fact a band of energy levels, a desirable feature as it makes the pumping more efficient and a larger part of the pumping input is converted into a useful output to produce population inversion. The energy levels involved in producing laser output are not necessarily single levels in all lasers. There could be multiple levels in the metastable state, in the lower energy state of the laser transition or in both states. This means that the laser has the ability to produce stimulated emission at more than one wavelength. Helium-neon and carbon

dioxide lasers are typical examples of this phenomenon. Figure 6.6 shows the energy level structure of a helium-neon laser.

Another important point worth mentioning here is that it is not always the active species alone that constitute the laser medium or laser material. Atoms or molecules of other elements are sometimes added with specific objectives. In some cases, such as in a helium-neon laser, the active species producing laser transition is the neon atoms. Free electrons in the discharge plasma produced as a result of electrical pumping input excite the helium atoms first as that can be done very efficiently. When the excited helium atoms collide with neon atoms, they transfer their energy to them. As another example, in a carbon dioxide laser the laser gas mixture mainly consists of carbon dioxide, nitrogen and helium. While

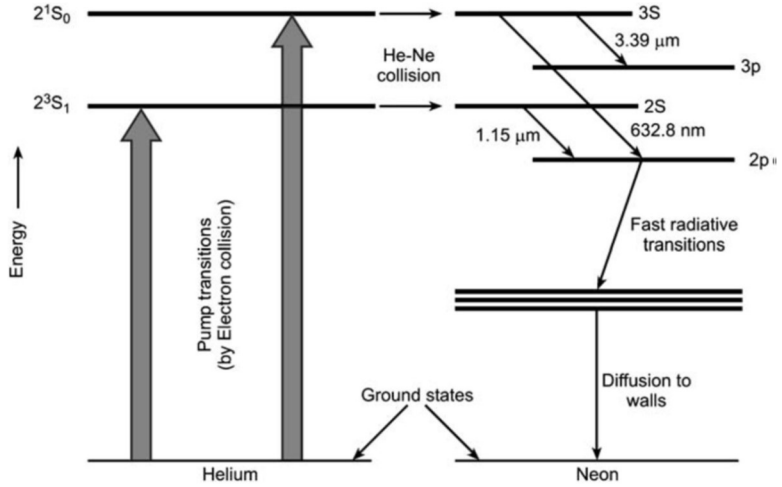

Fig 6.6 Energy level diagram of He-Ne laser.

Conclusion

Under thermodynamic equilibrium conditions, practically all atoms or molecules are in the lower level. A condition of population inversion is said to be achieved when the population N_2 of a higher energy level is greater than the population N_1 of a lower energy level. Population inversion is an essential condition for the laser action. There are two possible ways to produce population inversion. One is to populate the upper level by exciting extra atoms or molecules to the upper level. The other is to depopulate the lower laser level involved in the laser action. In fact, for a sustained laser action, it is important to both populate the upper level and depopulate the lower level. Energy level structure of the laser medium has an important bearing on the laser action and associated characteristics. All lasers operate as either three-level (e.g. ruby laser) or four-level lasers (e.g. Nd: YAG, He-Ne, CO_2). The transverse

modes basically tell us about the irradiance distribution of the laser output in the plane perpendicular to the direction of propagation or, in other words, along the orthogonal axes perpendicular to the laser axis. Commonly employed pumping mechanisms include optical pumping and electrical pumping. Other pumping mechanisms include by chemical reactions and electron beams.

Chapter VII
Laser Resonator and pumping mechanisms

7.1. Introduction

An optical resonator is an arrangement of mirrors that forms a standing wave in the cavity resonator for light waves. It is surrounding the gain medium and providing feedback of the laser light. Light confined in the cavity reflects multiple times producing standing waves for certain resonance frequencies. The standing wave

patterns produced are called modes; longitudinal modes differ only in frequency while transverse modes differ for different frequencies and have different intensity patterns across the cross-section of the beam.

7.2. Gain of Laser Medium

When we talk about the gain of the laser medium, we are basically referring to the extent to which this medium can produce stimulated emission. The gain of the medium is defined more appropriately as a gain coefficient, which is the gain expressed as a percentage per unit length of the active medium. When we say that the gain of a certain laser medium is 10% per centimeter, it implies that 100 photons with the same transition energy as that of an excited laser medium become 110 photons after travelling 1 cm of the medium length. The amplification or the photon multiplication offered by the medium is expressed as a function of the gain of the medium and the length of the medium, as described in Equation 1.2:

$$G_A = e^{\alpha x} \tag{7.1}$$

G_A = amplifier gain or amplification factor
α = gain coefficient
x = gain length
The above expression for gain can be re-written in the form:

$$G_A = (e^{\alpha})^x = (1 + \alpha)^x \text{ for } \alpha \ll 1 \tag{7.2}$$

Therefore, to a reasonably good approximation, we can write

$$\text{Amplification factor} = (1 + \text{gain coefficient})^{\text{length of medium}} \tag{7.3}$$

This implies that when the medium with a gain coefficient of 100% is excited and population inversion created, a single spontaneously emitted photon will become two photons after this spontaneously emitted photon travels 1 cm of the length of the medium. The two photons cause further stimulated emission as they travel through the medium. This amplification continues and the number of photons emitted by the stimulation process keeps building up just as the principal amount builds up with compound interest. The above relationship can be used to compute the amplification.

It would be interesting to note how photons multiply themselves as a function of length. For instance, although 10 photons become 11 photons after travelling 1 cm for a gain coefficient of 10% per centimeter, the number reaches about 26 for 10 cm and 1173 after travelling gain length of 50 cm, as long as there are enough excited species in the metastable state to ensure that stimulated emission dominates over absorption and spontaneous emission. On the other hand, it is also true that, for a given pump input, there is a certain quantum of excited species in the upper laser level. As the stimulated emission initially triggered by one spontaneously emitted photon picks up, the upper laser level is successively depleted of the desired excited species and the population inversion is adversely affected. This leads to a reduction in the growth of stimulated emission and eventually saturation sets in; this is referred to as gain saturation. Another aspect that we need to look into is whether the typical gain coefficient values that the majority of the active media used in lasers have been really good enough for building practical systems. Let us do a small calculation. If a 5 mW CW helium-neon laser were to operate for just 1 s, it would mean an equivalent energy of 5 mJ. Each photon of He-Ne laser output at 632.8 nm would have energy of approximately 3×10^{-19} J, which further implies that the above laser output would necessitate generation of about 1.7×10^{16} photons. With the kind of gain coefficient which the helium-neon laser plasma has, the required gain length can be calculated for the purpose. For any useful laser output, the solution therefore lies in having a very large effective gain length, if not a physically large gain length. If we enclose the laser medium within a closed path bounded by two mirrors, as shown in Figure 7.1, we can effectively increase the interaction length of the active medium by making the

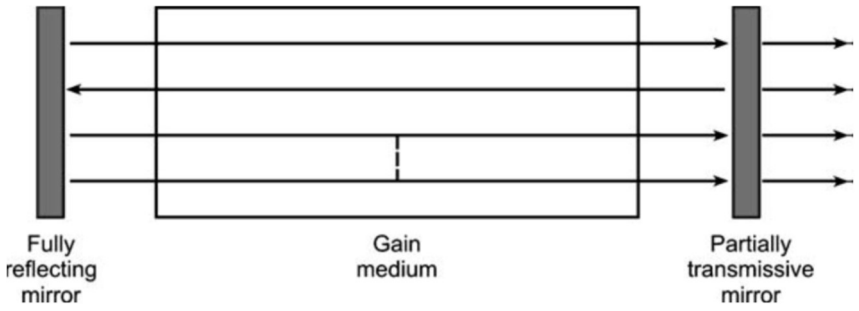

Figure 7.1 Lasing medium bounded by mirrors.

photons emitted by stimulated emission process back and forth. One of the mirrors in the arrangement is fully reflecting and the other has a small amount of

transmission. This small transmission, which also constitutes the useful laser output, adds to the loss component. This is true because the fraction of the stimulated emission of photons taken as the useful laser output is no longer available for interaction with the excited species in the upper laser level. The maximum power that can be coupled out of the system obviously must not exceed the total amount of losses within the closed path. For instance, if the gain of the full length of the active medium is 5% and the other losses such as those due to absorption in the active medium, spontaneous emission, losses in the fully reflecting mirror (which will not have an ideal reflectance of 100%) and so on are 3%, the other mirror can have at the most a transmission of 2%. In a closed system like this, the power inside the system is going to be much larger than the power available as useful output. For instance, for 1% transmission and assuming other losses to be negligible, if the output power is 1 mW the power inside the system would be 100 mW.

Example 7.1

Determine the gain coefficient in case of a helium-neon laser if a 50 cm gain length produces amplification by a factor of 1.1.

Solution

1. We have that $x = 50\ cm$ and the amplification factor $G_A = 1.1$.
2. The gain coefficient a can be computed from $G_A = e^{\alpha x}$ or $\alpha = (1/x) \ln G_A = (1/50) \ln 1.1 = 0.0019\ cm^{-1}$

7.3. Laser Resonator

The active laser medium within the closed path bounded by two mirrors as shown in Figure 7.1 constitutes the basic laser resonator provided it meets certain conditions. Resonator structures of most practical laser sources would normally be more complex than the simplistic arrangement of Figure 7.1. As stated in the previous section, with the help of mirrors we can effectively increase the interaction length of the active medium by making the photons emitted by the stimulated emission process travel back and forth within the length of the cavity. One of the mirrors in the arrangement is fully reflecting and the other has a small amount of transmission. It is clear that if we want the photons emitted as a result of the stimulated emission process to continue to add to the strength of those responsible for their emission, it is necessary for the stimulating and stimulated photons to be in phase. The addition of mirrors should not disturb this condition. For example, if the wave associated with a given photon was at its positive peak at the time of reflection from the fully

reflecting mirror, it should again be at its positive peak only after it makes a round trip of the cavity and returns to the fully reflecting mirror again. If this happens, then all those photons stimulated by this photon would also satisfy this condition. This is possible if we satisfy the condition given in Equation 7.4:

$$Round\ trip\ length = 2L = n\lambda \tag{7.4}$$

Where
L = length of the resonator
λ = wavelength
n = an integer
The above expression can be rewritten as

$$f = \frac{nc}{2L} \tag{7.5}$$

Where
c = velocity of electromagnetic wave
f = frequency

7.3.1. Longitudinal and Transverse Modes

The above expression for frequency indicates that there could be a large number of frequencies for different values of the integer *n* satisfying this resonance condition. Most laser transitions have gain for a wide range of wavelengths. Remember that we are not referring to lasers that can possibly emit at more than one wavelength (such as a helium-neon laser). Here, we are referring to the gain-bandwidth of one particular transition. We shall discuss in detail in Chapter 4 how gas lasers such as He-Ne and CO_2 lasers have Doppler-broadened gain curves. A He-Ne laser has a bandwidth of about 1400 MHz for 632.8 nm transition (Figure 7.2a) and a CO_2 laser has a bandwidth of about 60 MHz at 10600 nm (Figure 7.2b). It is therefore possible to have more than one resonant frequency, each of them called a longitudinal mode, simultaneously present unless special measures are taken to prevent this from happening. As is clear from Equation 7.5, the inter-mode spacing is given by $c/2L$. For a He-Ne laser with a cavity length of 30 cm for example, inter-mode spacing would be 500 MHz which may allow three longitudinal modes to be simultaneously present as shown in Figure 7.3a. Interestingly, the cavity length could be reduced

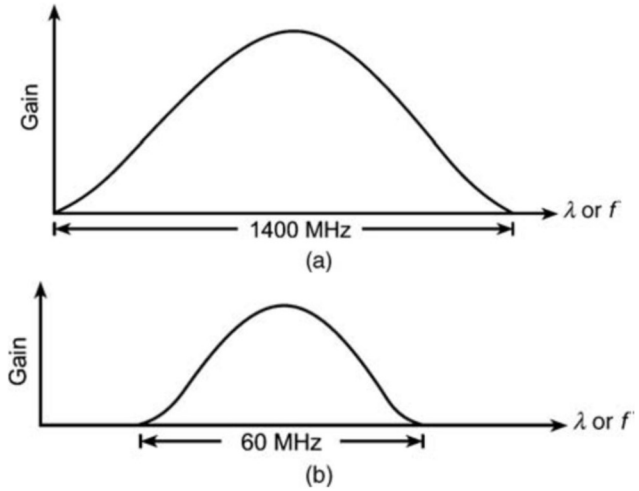

Figure 7.2 Gain-bandwidth curves for He-Ne and CO2 lasers.

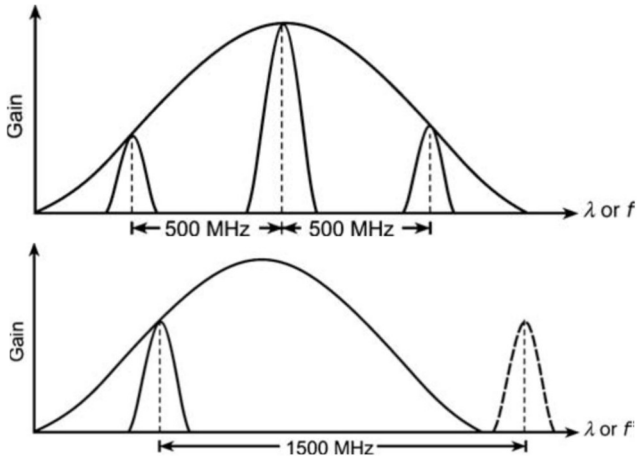

Figure 7.3 Longitudinal modes.

to a point where the inter-mode spacing exceeds the gain-bandwidth of the laser transition to allow only a single longitudinal mode to prevail in the cavity. For instance, a 10 cm cavity length leading to an intermode spacing of 1500MHz would allow only a single longitudinal mode (Figure 7.3b). However, there are other important criteria that also decide the cavity length. Another laser parameter that we are interested in and that is also largely influenced by the design of the laser resonator is the transverse mode structure of the laser output. We have already seen in the previous sections how the resonator length and the laser wavelength together decide the possible resonant frequencies called longitudinal modes, which can simultaneously exist. The transverse modes basically tell us about the irradiance distribution of the laser output in the plane perpendicular to the direction of propagation or, in other words, along the orthogonal axes perpendicular to the laser

axis. To illustrate this further, if the z axis is the laser axis, then intensity distribution along the x and y axes would describe the transverse mode structure. TEM_{mn} describes the transverse mode structure, where m and n are integers indicating the order of the mode. In fact, integers m and n are the number of intensity minima or nodes in the spatial intensity pattern along the two orthogonal axes. Conventionally, m represents the electric field component and n indicates the magnetic field component. Those who are familiar with electromagnetic theory should not find this difficult at all to grasp. Remember that transverse modes must satisfy the boundary conditions such as having zero amplitude on the boundaries. The simplest mode, also known as the fundamental or the lowest order mode, is referred to as TEM_{00} mode. The two subscripts here indicate that there are no minima along the two orthogonal axes between the boundaries. The intensity pattern in both the orthogonal directions has a single maximum with the intensity falling on both sides according to the well-known mathematical distribution referred to as the Gaussian distribution. The Gaussian distribution (Figure 7.4) is given by Equation 7.6:

$$I(r) = I_0 exp(-2r^2/w^2) \tag{7.6}$$

Where
$I(r)$ = intensity at a distance r from the centre of the beam.
w = beam radius at $1/e^2$ of peak intensity point, which is about 13.5% of the peak intensity.

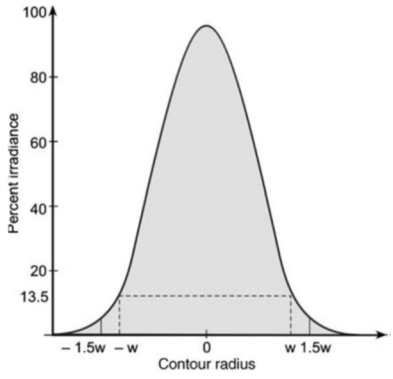

Figure 7.4 Gaussian distribution.

We also have

$$I_0 = \frac{2P}{\pi w^2} \tag{7.7}$$

Where

P = total power in the beam

Before we discuss the definite advantages that the operation at lowest order or fundamental modes TEM_{00} offers, we shall have quick look at higher-order modes and also how different transverse mode appear in relation to their intensity distributions. Figure 7.5 shows the spatial intensity distribution of the laser spot for various transverse mode structures of the laser resonator. Going back to the fundamental mode, we can appreciate that this mode has the least power spreading. To add to this, this mode has the least divergence; it has the minimum diffraction loss and therefore can be focused onto the smallest possible spot. The transverse mode structure is also critically dependent upon parameters such as laser medium gain, type of laser resonator and so on. There are established resonator design techniques to ensure operation at the fundamental mode. Often, lasers optimized to produce maximum power output operate at one or more higher-order modes. Also, lasers with low gain and stable resonator configuration can conveniently be made to operate at fundamental mode. Details are beyond the scope of this book, however.

Example 7.2

Given that the Doppler-broadened gain curve of a helium-neon laser with a 50-cm-long resonator emitting at 1.15 mm is 770 MHz, determine (a) inter-longitudinal mode spacing and (b) the number of maximum possible sustainable longitudinal modes.

Solution

Resonator length L= 50 cm. Therefore, inter-longitudinal mode spacing $= c/2L = 3 \times 10^{10}/100 = 300\ MHz$.

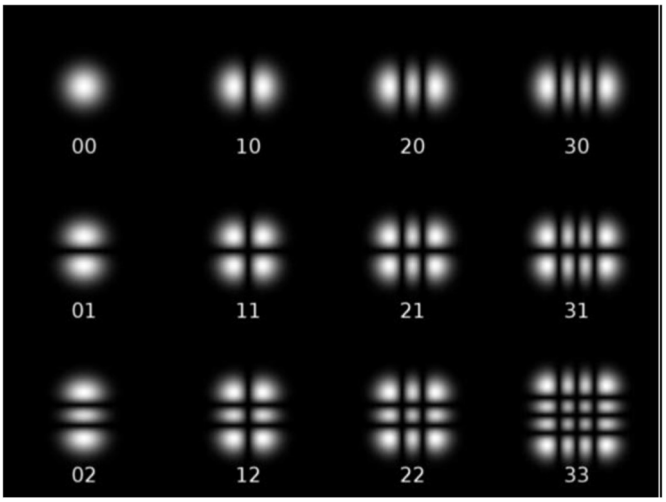

Figure 7.5 Spatial intensity distribution for various transverse modes.

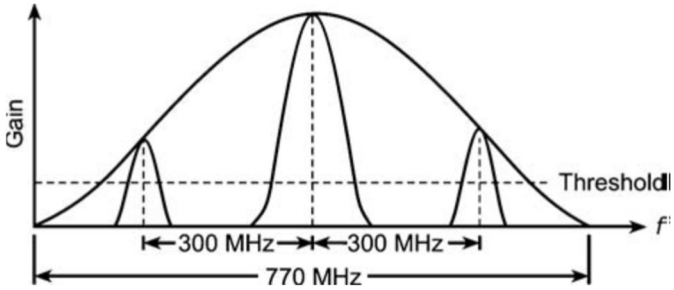

Figure 7.6 Diagram for Example 7.2.

Width of Doppler-broadened gain curve¼770 MHz. The number of longitudinal modes possible within this width=3 (Figure 7.6).

7.3.2. Types of Laser Resonators

According to the type of end mirrors used and the inter-element separation, which largely dictates the extent of interaction between the emitted photons and the laser medium and also the immunity of the laser resonator to misalignment of end components, the resonators can be broadly classified as stable and unstable resonators. A stable resonator is one in which the photons can bounce back and forth between the end components indefinitely without being lost out the sides of the components. Due to the focusing nature of one or both components, the light flux remains within the cavity in such a resonator. A plane-parallel resonator (Figure 7.7) in which both end components are plane mirrors and are placed precisely at right angles to the laser axis is a stable resonator. In practice, however, this is not true. A slight misalignment of even one of the mirrors would ultimately lead to light flux escaping the laser cavity after several reflections from the two mirrors. Nevertheless,

such a resonator encompasses a large volume of the active medium. It is not used in practice, as it is highly prone to misalignment.

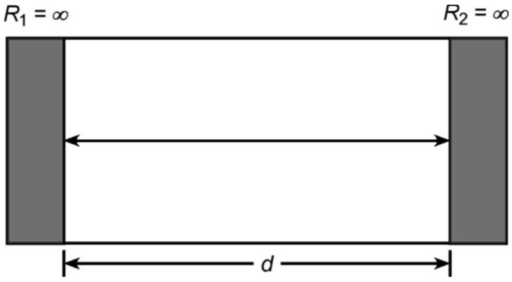

Figure 7.7 Plane-parallel resonator.

This problem can be overcome by using one plane and one curved mirror, as is the case for hemispherical and hemifocal resonators shown in Figure 7.8a and b, respectively, or two curved mirrors, as is the case for concentric and confocal resonators shown in Figure 7.9a and b, respectively. Although the problem of sensitivity of the plane-parallel resonator to misalignment of cavity mirrors is largely overcome by the use of different stable resonator configurations discussed above (Figures 7.8 and 7.9), not all of them have emitted photons interacting with a large volume of the excited species, which is also equally desirable. It is also true that in the case of low-gain media with consequent very low transmission output mirrors, the photons travel back and forth a large number of times within the cavity before their energy appears at the output. This makes the resonator alignment more critical. That is why a plane-parallel resonator will never be the choice for a low-gain laser medium.

On the other hand, in a high-gain medium a certain amount of light flux leakage can be tolerated. This fact is made use of in an unstable resonator configuration, which otherwise achieves interaction of the emitted photons with a very large volume of the excited species. Figure 7.10 shows one possible type of unstable resonator. Note that photons escape from the sides of the mirror after one or two passes within the cavity. This light leakage, which also constitutes the useful laser output, is more than compensated for by a high-gain medium and large interaction volume. Further, since the photons have to make

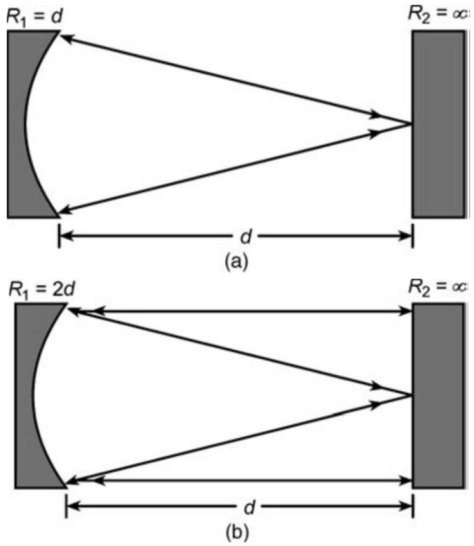

Figure 7.8 (a) Hemispherical resonator and (b) hemifocal resonator.

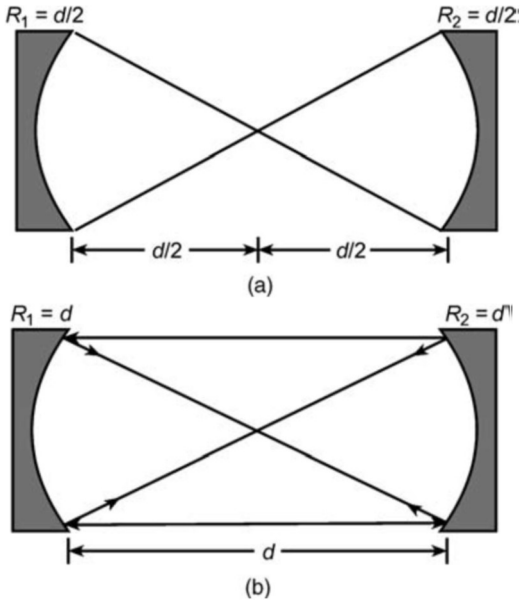

Figure 7.9 (a) Concentric resonator and (b) confocal resonator.

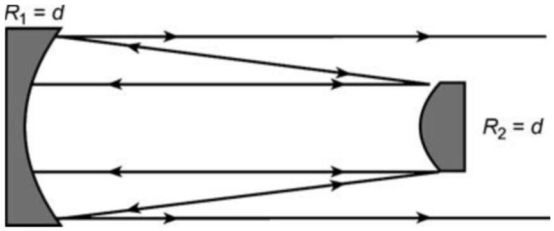

Figure 7.10 Unstable resonator.

relatively fewer passes within the cavity as compared to a low-gain stable resonator configuration before drifting out, the alignment becomes much less critical.

7.4. Pumping Mechanisms

By pumping mechanism, we mean the mechanism employed to create population inversion of the lasing species. Commonly employed pumping mechanisms include:

1. optical pumping;
2. electrical pumping; and
3. other mechanisms such as pumping by chemical reactions, electron beams and so on.

One aspect that is common to all pumping mechanisms is that the pumping energy/power must be
greater than the laser output energy/power. When applied to optical pumping, it is obvious that the
optical pump wavelength must be smaller than the laser output wavelength. This has to be true as the

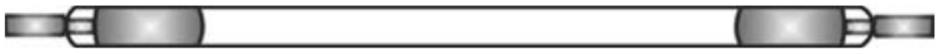

Figure 7.11 Linear flash lamps.

lasing species are first excited to the topmost level from where they drop to the upper laser level. Since the energy difference between the ground state and the topmost pump level is always greater than the energy difference between the two laser levels, the wavelength of the pump photon must be less than the wavelength of the laser output. Another aspect that is common to all schemes is that pumping efficiency largely affects the overall laser efficiency. For instance, if the energy difference for the pump transition is much greater than that of the laser transition, the laser efficiency is bound to be relatively poorer. An argon-ion laser is a typical example. Yet another aspect that is common to all pumping mechanisms is that the topmost pump level is not a single energy level but rather a band of closely spaced energy levels with allowed transitions to a single and, in some cases, more than one metastable level. When applied to optical pumping, this allows the use of optical sources such as flash lamps with broadband outputs.

7.4.1. Optical Pumping

Optical pumping is employed for those lasers that have a transparent active medium. Solid-state and liquid-dye lasers are typical examples. The most commonly used pump sources are the flash lamp in the case of pulsed and the arc lamp in the case of continuous-wave solid-state lasers. Flash lamps are pulsed sources of light and are widely used for the pumping of pulsed solid-state lasers. These are available in a wide range of arc lengths (from a few centimeters to as large as more than a meter, although arc length of 5–10 cm is common), bore diameter (typically in the range of 3–20 mm), wall thickness (typically 1–2 mm) and shape (linear, helical). Figures 1.22 and 1.23 depict the constructional features of typical linear (Figure 7.11) and helical (Figure 7.12) flash lamps.

Flash lamps for pumping solid-state lasers are usually filled with a noble gas such as xenon or krypton at a pressure of 300–400 torr. Two electrodes are sealed in the envelope that is usually made of quartz. An electrical discharge created between the electrodes leads to a very high value of pulsed current, which further produces an intense flash. The electrical energy to be discharged through the lamp is stored in an energy storage capacitor/capacitor bank. Xenon-filled lamps produce higher radiative output for a given electrical input as compared to krypton-filled lamps. Krypton however offers a better spectral match, more so with Nd:YAG. That is, the emission spectrum of a krypton flash lamp is better matched to the absorption spectrum of Nd:YAG. Emission spectra in the case of xenon- and krypton-filled lamps are depicted by Figures 7.13 and 7.14, respectively. The absorption spectrum of a Nd:YAG laser is given in Figure 7.15.

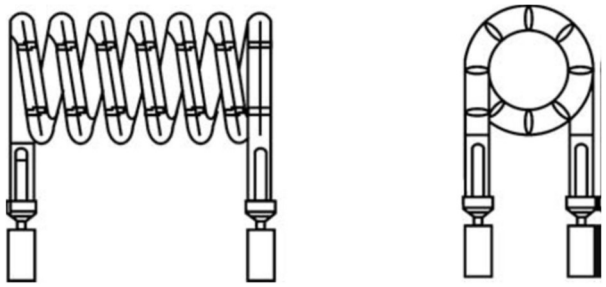

Figure 7.12 Helical flash lamp.

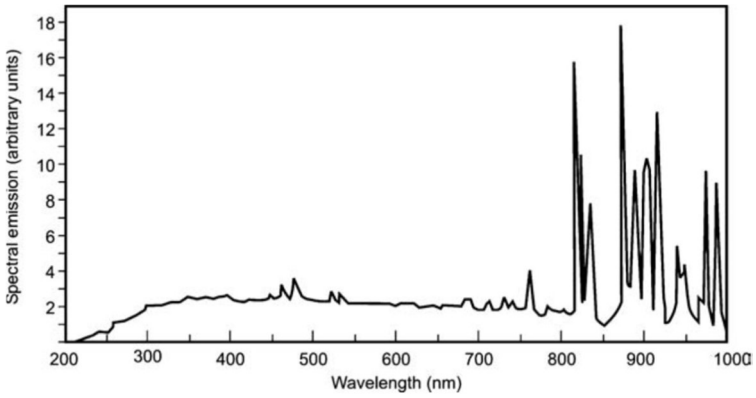

Figure 7.13 Emission spectrum of xenon-filled flash lamp.

Major electrical parameters include the flash lamp impedance parameter, maximum average power, maximum peak current, minimum trigger voltage and explosion energy. Impedance characteristics of a flash lamp are extremely important as they determine the energy transfer efficiency from energy storage capacitor, where it is stored, to the flash lamp. Table 1.1 gives typical values of various characteristic parameters of xenon-filled and krypton-filled pulsed flash lamps from Heraeus Noble light Ltd. The type numbers chosen for the purpose include both air-cooled as well as liquid-cooled flash lamps of different bore diameter and arc length. This assortment of flash lamps highlights the variation of the electrical parameters with bore diameter and arc length for a

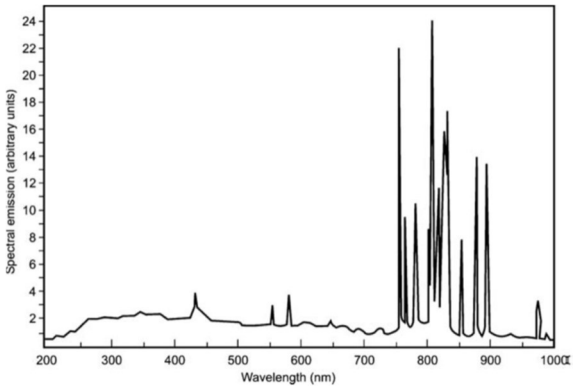

Figure 7.14 Emission spectrum of Krypton-filled flash lamp.

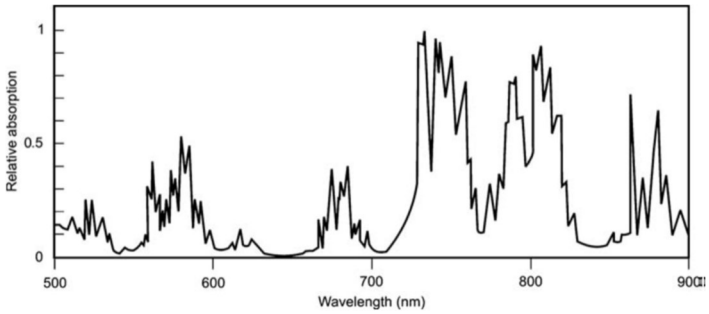

Figure 7.15 Absorption spectrum of Nd:YAG.

Conclusion

The gain of the medium is defined as gain coefficient, which is the gain expressed as a percentage per unit length of the active medium. The gain of the laser medium refers to the extent to which this medium can produce stimulated emission. The amplification or the photon multiplication offered by the medium is expressed as a function of the gain of the medium and the length of the medium by: $\text{Amplification} = (1 + \text{gain coefficient})^{\text{length of medium}}$. A resonator is the active laser medium within the closed path bounded by two mirrors, providing it meets certain conditions. One of the mirrors in the arrangement is fully reflecting and the other has a small amount of transmission. A laser resonator satisfies: round trip length $= 2L = nl$ where L, n and l denote length of the resonator, an integer and wavelength, respectively. The resonators can be broadly classified as stable and unstable resonators. A stable resonator is one in which the photons can bounce back and forth between the end components indefinitely without being lost out the sides of the components. In unstable resonator photons escape from the sides of the mirror after one or two passes within the cavity. An unstable resonator is usually chosen with laser media that have a very high gain, as alignment in this resonator type is much less critical. It is possible to have more than one resonant frequency (each referred to as a longitudinal mode) to be simultaneously present unless special measures are taken to prevent this from happening. The intermode spacing is given by $c/2L$.

References

[1] Optical Fiber Communications Principles and Practice (3rd Edition) (John Senior)
[2] Dielectrics in electric fields (Raju, Gorur G)
[3] Fiber Optic Communications Fundamentals and Applications Shiva Kumar and M. Jamal Deen
[4] Fiber-Optic Communication Systems (Govind P. Agrawal)
[5] Fiber-Optic Communication Systems, 4th Edition (Wiley Series in Microwave and Optical Engineering) (Govind P. Agrawal)
[6] Fiber-Optic Communications Technology (3rd Edition) (Djafar K.Mynbaev, Lowell L. Scheiner)
[7] Fundamentals of optical waveguides (Katsunari Okamoto)
[8] Laser Beam Propagation in Nonlinear Optical Media (Shekhar Guha, Leonel P. Gonzalez)
[9] Nonlinear Fiber Optics (Agrawal, Govind)
[10] Nonlinear Optics (Robert W. Boyd)
[11] Optical Fiber Communications (Gerd Keiser)
[12] Optical Fiber Communications Principles and Practice (3rd Edition) (John Senior)
[13] Practical Optics (Naftaly Menn)